Thiolutin has complex effects in vivo but is a direct inhibitor of RNA Polymerase II in vitro

Chenxi Qiu[1,6], Payal Arora[1,2], Indranil Malik[1,7], Amber J. Laperuta[3,8], Emily M. Pavlovic[4,9], Scott Ugochukwu[5], Mandar Naik[1,10], Craig Kaplan[2]

[1] Department of Biochemistry and Biophysics, Texas A&M University, College Station, TX 77843, USA
[2] Department of Biological Sciences, University of Pittsburgh, Pittsburgh, PA 15260, USA
[3] Stevenson University, Stevenson, MD 21153, USA
[4] Earlham College, Richmond, IN 47374, USA
[5] Texas State University, San Marcos, TX 78666 USA
[6] Present Address: Department of Genetics, Harvard Medical School, Boston, MA 02115, USA
[7] Present Address: Department of Biotechnology, Indian Institute of Technology Hyderabad, Sangareddy, Telangana, India
[8] Present Address: Department of Biological Sciences, University of Pittsburgh, Pittsburgh, PA 15217, USA
[9] Present Address: University of Minnesota-Duluth, Duluth, MN 55812, USA
[10] Present Address: Department of Molecular Pharmacology, Physiology and Biotechnology, Brown University, Providence, RI 02912, USA

Abstract

Thiolutin is a natural product transcription inhibitor with an unresolved mode of action. Thiolutin and the related dithiolopyrrolone holomycin have Zn^{2+}-chelation activity and previous studies have concluded that RNA Polymerase II (Pol II) inhibition *in vivo* is indirect. However, negative results for direct transcription inhibition of Pol II are in contrast to classical studies showing thiolutin inhibits Pol I, II, and III in yeast extract fractions. Here, we present chemicogenetic and biochemical approaches to investigate thiolutin's mode of action in *Saccharomyces cerevisiae*. We identify mutants that alter sensitivity to thiolutin. We provide genetic evidence that thiolutin causes oxidation of thioredoxins *in vivo* and that thiolutin both induces oxidative stress and alters not just Zn^{2+} but potentially also Cu^{2+} and Mn^{2+} homeostasis *in vivo*. Finally, we show direct inhibition of RNA polymerase II (Pol II) transcription by thiolutin *in vitro*. Inhibition requires both Mn^{2+} and appropriate reduction of thiolutin. Thio/Mn^{2+} inhibition is abrogated when template DNA is pre-bound to Pol II or when excess DTT is present, and renders Pol II pause prone in elongation if thiolutin inhibition of initiation is bypassed. We find that thiolutin effects in cells are complex, unlikely to arise solely due to Zn^{2+} chelation.

Introduction

Thiolutin is a historically used transcription inhibitor with potentially multiple modes of action. Thiolutin one of the microbially produced dithiolopyrrolone compounds that feature an intra-molecular and redox-sensitive disulfide bond (1,2). Holomycin is another notable compound in this class. These compounds are thought to be pro-drugs whose anti-microbial action requires reduction of the intramolecular disulfide. Thiolutin has been shown to inhibit bacterial and eukaryotic transcription *in vivo* and has been used to study mRNA stability in multiple species (3-6). However, the mode of action of thiolutin for transcription inhibition remains unclear and complicated (discussed below). In addition, thiolutin appears to affect multiple cellular pathways, including glucose metabolism, Tor signaling (7), Hog/MAPK pathway signaling, P body formation, mRNA degradation, the oxidative stress response, and proteasome activity (7-11).

Recent progress has suggested that both thiolutin and holomycin act as redox-sensitive Zn^{2+} chelators, providing an explanation for their diverse cellular effects (1,11-13). It has been demonstrated *in vitro* that thiolutin and holomycin can be reduced by strong reductants such as DTT or TCEP (1,11) and that reduced thiolutin and holomycin can chelate Zn^{2+} (11,12). The Zn^{2+} chelating activity explains multiple thiolutin induced phenotypes, including alteration of glucose metabolism and proteasome inhibition through inhibition of Zn^{2+}-specific metalloproteins (8,11). In addition, two observations suggest a possible mechanism for the thiolutin-induced expression of oxidative stress response genes (9). First, thiolutin and holomycin appear to require reduction for their activity, and reduction of thiolutin could in turn oxidize the cellular reductant or reducing proteins (1,12). Second, reduced holomycin can be spontaneously oxidized by molecular oxygen, suggesting that holomycin may be a redox cycling compound (14,15) and cause accumulation of reactive oxygen species (ROS). Whether thiolutin can act as a redox cycler has not yet been tested, and the cellular reductant(s) for thiolutin or holomycin remain complicated. Earlier reports indicated that glutathione does not reduce holomycin *in vitro* (1). Recently, levels of glutathione in the range of those in vivo have been shown to reduce multiple dithiolopyrrolones in vitro and to activate Zn^{2+}-chelating activity, consistent with these natural products being pro-chelators requiring reduction (16). Together, the Zn^{2+} chelating and redox activities are consistent with previously observed diversity in thiolutin-induced phenotypes, though transcription inhibition has not been easily explained. Both thiolutin and holomycin have been observed to be inert against RNAPs under conditions where either should be able to chelate Zn^{2+}. Furthermore, it is not clear how Zn^{2+} chelation would be expected to inhibit transcription. In light of these negative results, transcription inhibition by dithiolopyrrolones was concluded to be a secondary outcome of inhibition of a distinct target, such as the proteasome. For example, thiolutin elicits removal of zinc from Rpn11, an essential deubiquitinase required for the proteasomal processing of ubiquitinated substrates (11,12).

There is extensive evidence for thiolutin inhibition of transcription *in vivo* in multiple species (17-19), though from *in vitro* studies it has been concluded that it inhibits prokaryotic and eukaryotic RNAPs differently. Thiolutin inhibited all three partially purified yeast RNAPs *in vitro* (20), but failed to inhibit all tested prokaryotic RNAPs *in vitro* (18,19,21). Similar RNAP inhibition *in vivo* with lack of inhibition *in vitro* has been observed for holomycin (12,22). The recently reported lack of thiolutin inhibition for all three fully purified yeast RNAPs has added further confusion (11). Therefore, our current state of understanding is that thiolutin and holomycin do not appear to inhibit prokaryotic or fully purified eukaryotic RNAPs, suggesting indirect modes of *in vivo* transcription inhibition. However, without comprehensive assessment of the experimental parameters for different transcription assays, it seems difficult to rule out direct mechanisms of action for thiolutin on eukaryotic RNAPs, as recent work does not satisfactorily explain why thiolutin inhibited all three partially purified yeast RNA polymerases *in vitro* (20), and how

thiolutin inhibited RNAPs prior to template addition, but did not inhibit the template DNA bound RNAPs (20). This critical order-of-addition requirement for treatment prior to DNA addition is reminiscent of RNAP switch region inhibitor behavior (23,24) and is consistent with inhibition of a specific and early step in transcription, in contrast to Zn^{2+} chelation.

We can imagine a number of possibilities to reconcile the existing data. First, thiolutin may target a secondary protein, which is present *in vivo* and in partially purified RNA polymerase fractions (20) but not others (11,19,21). Second, as predicted (11,12), thiolutin may act as a prodrug that is activated *in vivo* and under the *in vitro* conditions of the early report (20) but not in assays used by others (11,19,21). To further investigate the mode of action of thiolutin, we have undertaken multiple approaches to screen for thiolutin resistant and sensitive mutants, as similar studies have contributed to understanding of modes of actions of many compounds (25-27), including holomycin (12). We identify a drug efflux pump functioning in thiolutin resistance and demonstrate that thiolutin treatment appears to induce oxidative stress. We propose that thiolutin likely induces the oxidative stress via oxidizing thioredoxins and possibly also through redox-cycling. In addition, we confirm that reduced thiolutin directly interacts with Zn^{2+} *in vitro*, consistent with the recent reports on holomycin and thiolutin using different approaches (11,12). We also suggest that thiolutin alters cellular Zn^{2+} homeostasis in yeast similar to holomycin's effects in *E.coli* (12) but also find complex interactions with Co^{2+}, Cu^{2+} and Mn^{2+} that are distinct from those of 1,10-phenanthroline, another class of Zn^{2+} chelator that inhibits transcription *in vivo* but has been described as an inhibitor *in vitro* through a Cu-chelate (28).

Finally, we have revisited *in vitro* biochemical studies with thiolutin and Pol II. We find that thiolutin indeed inhibits Pol II but critically requires the presence of small amounts of Mn^{2+}, providing an explanation for disparate results across studies. First, DNA bound Pol II is resistant to thiolutin inhibition, recapitulating Tipper's early study (20). Second, though thiolutin appears to inhibit a very early step in Pol II transcription, when initiation is bypassed by use of specific nucleic acid templates, thiolutin-treated Pol II exhibits pause-prone, slow elongation. Third, high DTT reverses the thiolutin inhibition, suggesting involvement of disulfide bond or redox sensitive covalent chemistry in inhibition. We find that thiolutin appears to inhibit initiation *in vivo* and reduces Pol II occupancy near promoters across many yeast genes. Elongation of Pol II on genes also appears altered in that Pol II does not appear to completely run off longer genes as it would if elongation were unaltered. We propose that thiolutin inhibits Pol II transcription directly through a novel mechanism distinct from known Pol II transcription inhibitors.

Material and Methods

Yeast strains and reagents

Yeast strains and primers used are listed in Table S2. *YAP1* C-terminal tagging with EGFP and gene deletion strains were constructed as described (29,30). Chemicals were commercially obtained from the following: Cayman Chemical (Thiolutin), Gold Biotechnology (DTT, TCEP, 5FOA), Sigma ($MnCl_2$), JT Baker ($ZnCl_2$), BDH Chemicals ($MgCl_2$).

Variomics screens

Two separate pools of diploid Variomics libraries were gifts from Dr. Xuewen Pan: one for non-essential and the other for essential genes (31). The pooled diploid Variomics libraries were grown, sporulated and selected for haploid Variomics libraries as described (31). Haploid Variomics libraries were subsequently used for the genetic screens. To convert the Variomics libraries into plasmid-free deletion libraries, pooled Variomics libraries (diploid for essential genes and haploid for non-essential genes) were grown in liquid SC media and plated on SC+5FOA plates to select against the mutants with the *URA3* plasmids containing the

Variomics mutations. The diversity of the libraries were confirmed by deep sequencing of barcodes ("uptags" and "downtags") flanking the deletion cassettes.

For manual screening of variomics libraries, about 1-3×10^7 cells were plated on SC+10μg/mL thiolutin plates, and the potential thiolutin resistant candidates were restruck out on SC+10μg/mL thiolutin plates to validate the resistance. The plasmids from the validated resistant candidates were subsequently recovered for Sanger sequencing to identify putative resistance-conferring variants. We subsequently tested dominance for the repeatedly isolated candidates. The recovered plasmids from all reproducibly isolated candidates were transformed into the wild-type (CKY457) strain, and thiolutin sensitivity for transformants was phenotyped and compared to the empty vector control.

For high-throughput screens, Variomics libraries were screened on plates, while deletion libraries were screened in liquid, as previously described (25,26,31), and three independent screens (biological replicates) were performed. For Variomics screens, each library was screened on SC-URA+DMSO, SC-URA+8μg/mL thiolutin or SC-URA+10μg/mL plates. Each biological replicate was screened on 9 plates (6×10^7 cells/plate) for 3 days, and cells were scraped to screen for an additional set of 9 plates for 3 days (6×10^7 cells/plate). Deletion libraries were grown in liquid SC media to 3×10^7 cells/mL and diluted in SC+3μg/mL thiolutin (for haploid non-essential gene deletion library) or SC+4μg/mL thiolutin (for diploid essential gene deletion library) to grow for 20 generations. During the selection, the cells were diluted to 1×10^6 cells/mL every five generations to maintain cultures in log phase. For both screens, yeast cells were pooled, and genomic DNA was prepared using a YeaStar Genomic DNA kit (Zymo Research) for subsequent PCR amplification of barcode regions. Amplicons were sequenced by illumina Hiseq2500 in rapid mode. The sequencing reads are deposited in the SRA under the Bioproject PRJNA725683.

Bar-seq data processing

Sequencing reads are mapped to the re-annotated barcode sequences (25) using Bowtie2 (32) (version 2.2.4) with the -N flag set to 0 and the --no-unal flag to suppress unaligned reads for further analyses. Bowtie2 outputs were written into SAM format and further extracted using Samtools (version 1.3.1) (33). Barcode sequences shorter than 15nts or were mapped to multiple reference barcodes were discarded. On average, 98% of sequencing reads were uniquely mapped.

As with Robinson *et al.* (34), we filtered out barcodes with lower than 100 total reads across all samples, since low count barcodes across all conditions were likely from sequencing errors and did not exist. In addition, mutants with less than 20 reads in both treated and the corresponding untreated controls are further filtered out, to exclude large changes from a small amount of reads with low confidence.

Following Robinson *et al.* (34), we added 1 pseudo-count to each barcode count to avoid division by 0, and performed TMM normalization using the edgeR package (version 3.12.1) (35). For differential abundance analyses, we used the edgeR to compute mutant specific dispersions, p-value and log transformed abundance changes using exactTest function (default setting). The transformed data were subsequently subjected to differential abundance analyses and clustering analyses. Differential abundance analyses were performed independently for the uptag and downtag sequences, and reproducibility between uptag and downtag data was assessed with Pearson correlation in R. Hierarchical clustering of the thiolutin phenotypic profile to an existing drug response profile for yeast mutants, consisting of 3356 compounds (26) was performed in Cluster 3.0 (36), using centered correlation and complete linkage.

Mutants with significantly altered abundance ($p<0.01$) were subjected to gene-ontology (GO) analyses as previously reported (26). In brief, all three GO categories, including biological processes (BP), Molecular Function (MF) and Cellular components (CC), were included in our analyses. Following the previous report (26), BP and MF GO terms that are too specific (present in less than 5 genes) or too generic (present in greater than 300 genes) were excluded, although smaller GO term groups were allowed for protein complexes (more than 2 genes) and larger groups (greater than 300 genes) were allowed for cellular components. We computed the GO term enrichment analyses for the significantly resistant or sensitive mutants ($p<0.01$) using hypergeometric test in R (version 3.2.2, physer function, default setting). Raw counts and p-value for each GO term were reported.

A series of quality controls were performed on the reproducibility among biological replicates, consistency between the two barcodes on each gene deletion (uptag and downtag) for the same strain, common and distinct properties between Variomics and Deletion libraries following a well-established statistical analysis pipeline. A subset of the statistically significant resistant or sensitive mutants were further validated by re-constructing the deletion strain for individual phenotyping.

Visualization of Yap1 localization under fluorescence microscopy

Microscopy experiments were performed as previously described (37). In brief, CKY2038 was grown to mid-log (1-2×10^7 cells/mL) in SC liquid media and added to the ConA treated perfusion chamber gasket (ThermoFisher, 4 chamber: 19 × 6mm) for treatment at indicated conditions (SC+1% DMSO, SC+10μg/mL Thiolutin, SC+10μg/mL Holomycin or SC+0.4mM H_2O_2) under the fluorescence microscope. The procedure to prepare the chamber and the microscope setting were the same as previously described.

Glutathione quantitation assays

WT yeast (CKY457) cultures were grown (in YPD at 30˚C) until mid-log phase (~2×10^7 cells/mL), washed and resuspended in the indicated conditions (YPD+1% DMSO, YPD+10μg/mL Thiolutin or YPD+10μg/mL Holomycin). The suspended cultures were grown at 30˚C for one hour, and 5×10^7/mL cells were subject to glutathione (GSH) quantitation. The active and total GSH levels were quantified using the GSH detection kit from Arbor Assays (K006-F5) following the manual. The glutathione disulfide (GSSG) level was calculated by (Total GSH - Active GSH)/2.

UV-Vis assays

Thiolutin reduction and Zn^{2+} chelation reactions were performed in 250μL reactions with 50μM Thiolutin, 50μM $ZnCl_2$ and 100mM potassium phosphate buffer (pH=6.5), as previously described (1). Mn^{2+} chelation reactions and relevant controls were performed under almost identical conditions except for the 100mM Tris buffer (pH=8) to keep consistent pH with the *in vitro* transcription assays. Each reaction had 250μL final volume and was quantified in Nanodrop 2000c spectrophotometer using UV-transparent cuvettes.

Growth, viability and canavanine resistance assays

Phenotyping of mutants using plate assays were performed as previously described, with indicated addition of chemicals (38,39). Yeast liquid growth curve assays with Tecan Infinite F200 plate readers were performed as previously described (37). For viability assays and canavanine resistance assays, WT yeast strain CKY457 was grown in YPD until mid-log (1-2×10^7 cells/mL), washed and treated with the indicated conditions (YPD, YPD+3μg/mL thiolutin, YPD+5μg/mL thiolutin and YPD+10μg/mL thiolutin) for an hour. The viability was quantified by

staining the yeast cells in 0.1% Trypan blue staining (GE Healthcare Life Sciences, Catalog Number SV30084.01) for 3 mins, and the viability was quantified by counting the fraction of unstained yeast cells under the microscope. At least 300 yeast cells were counted in each repeat. Canavanine resistance frequency was quantified by plating the culture onto YPD and SC-Arg+60μg/mL canavanine plates and dividing the number of canavanine resistant colonies by the number of viable colonies on YPD plates. Three experimental replicates were performed.

Pol II transcription activity assays

Pol II was purified using a strain expressing Rpb3 tagged with tandem-affinity tag (TAP), following a procedure as previously described (40). For initiation experiments DTT was removed from the Pol II buffer prior to the assay using Zeba spin desalting column (Thermo Scientific), though in later experiments this was found to be unnecessary.

Standard ssDNA transcription assays were performed in the *in vitro* transcription buffer (20mM Tris-HCl pH8, 40mM KCl, 5mM $MgCl_2$). Each reaction had ~0.5 pmol Pol II, 2μg denatured sheared salmon sperm DNA as the template and 200μM NTPs except 9μM cold NTP for labeling with that species (UTP or CTP), 1μM radioactive α-^{32}P UTP or CTP (800 Ci/mmol, Perkin-Elmer) as substrates. The concentration of thiolutin, reductants (DTT or TCEP) and $MnCl_2$ varies among the experiments (indicated in each figure). In general, 5 μl pre-treatment reactions including DMSO or thiolutin (at 2X final treatment concentration, from 7.5 μg/mL to 60 μg/mL in DMSO), +/- $MnCl_2$ at specified concentration, and DTT (1-2X molar equivalent to thiolutin) were composed and incubated for 5 minutes at room temperature. To these reactions Pol II was added (with or without pre-binding to DNA) in an equal volume of 2X transcription buffer, yielding 10 μl reactions in 1X transcription buffer for thiolutin treatment. These reactions were incubated for 20 minutes at room temperature. Transcription was initiated by addition of 5 μl DNA/NTP (or just NTP mix in case of pretreatment) and incubated at room temperature for 30 minutes then stopped with stop buffer (10M Urea, 5mM EDTA in TBE). DTT reversal of thiolutin inhibition was accomplished by adding 2 μl 60 mM DTT to 8 μl Pol II treatment reaction at the end of the 20 minute treatment, prior to addition of NTPs/DNA. Transcripts were separated from unincorporated α-^{32}P NTPs on 10% acrylamide/7M urea/TBE gels and visualized with a Bio-Rad Pharos Phosphorimager or GE Typhoon Imager. In vitro transcription elongation assays were performed as previously described (40), with modifications of time in the figure. 5μl reactions comprising 5 pmol Pol II, 40 μg/mL thiolutin in DMSO or DMSO alone, 875 μM $MnCl_2$, equimolar DTT to thiolutin, 1X transcription buffer, and 3.75 μg BSA were incubated for 20 minutes at room temperature and incubated with 2.5 μl annealed transcription scaffold as described. After 5 minutes, non-template strand was added for an additional 5 minute incubation. Thiolutin-treated Pol II+scaffold was then diluted with additional 1X transcription buffer, $MnCl_2$, thiolutin, while untreated Pol II+scaffold was diluted with thiolutin containing buffer (made fresh) or control buffer with DMSO. After 20 additional minutes at room temperature, reactions proceeded exactly as described in (40).

ChIP-qPCR and ChIP-seq

(*RPB3::3XFLAG::kanMX4*) subunit of Pol II was used for chromatin immunoprecipitation (ChIP). For in vivo elongation assays, Pol II occupancy over a constitutive promoter-driven reporter (*TEF1p::YLR454W*) was determined after treating the cells with thiolutin. Yeast were grown in SC media to mid-log (1X10^7 cells/mL) and treated with 10 μg/mL thiolutin for 2, 4, 8 or 10 mins (ChIP-qPCR) or for 1, 2, 4, or 8 mins (ChIP-seq), cross-linked with 1% formaldehyde solution (1% formaldehyde, 10mM NaCl, 100μM EDTA and 5mM HEPES-KOH, pH 7.5) for 20 minutes and quenched by 3M glycine (final concentration 360mM) for 5 minutes. ChIP- qPCR was performed as described previously (37). In brief, cross-linked cells were disrupted by bead beating and cell lysate was centrifuged at 1500 rpm for 1 min at 4˚C to remove cell-debris,

292 followed by centrifugation of chromatin pellets, subsequent washing of pellets (twice) with 1 ml
293 FA buffer (50 mM HEPES-KOH pH 7.5, 300 mM NaCl, 1 mM EDTA, 0.1% Triton X-100, 0.01%
294 sodium deoxycholate, 0.1% SDS and 1 mM PMSF) at 14000 rpm for 20 min at 4˚C. Chromatin
295 for ChIP-seq was washed one additional time in special FA buffer lacking SDS and sodium
296 deoxycholate. Chromatin pellets were sonicated using a Diagenode Bioruptor (ChIP-qPCR, 45
297 cycles – 3 × 15 cycles; 30 s ON/45 s OFF) or a Diagenode Bioruptor Pico (ChIP-seq, 20 cycles;
298 30 s ON/30-50 s OFF) and used for IP with anti-FLAG antibody (FLAG M2 magnetic beads,
299 Sigma-Aldrich). For ChIP-seq, 1100 µg of chromatin material as determined by BCA assay
300 (Thermo Fisher) was used for each IP with addition of 110 µg *S. pombe* spike-in chromatin from
301 CKP025 (*h- ura4-D18 rpb3+::6gly-3Flag-ura4+*). Concentration of SDS in IP for ChIP-seq after
302 addition of *S. pombe* chromatin was 0.1% and concentration of sodium deoxycholate was
303 0.01%. SDS and sodium deoxycholate were omitted from all washes for ChIP-seq IPs as they
304 reduce efficiency of FLAG M2 antibody (MilliporeSigma). 10% of the total IP material was used
305 as input. Input or immunoprecipitated DNA was purified by standard phenol–chloroform
306 extraction and ethanol precipitated with pellet paint (MilliporeSigma) or glycoblue
307 (ThermoFisher). Immunoprecipitated DNA and 10% of corresponding input DNA (1:10 diluted)
308 were used for qPCR with SsoAdvanced Universal SYBR Green supermix (Bio-Rad) using CFX
309 96 (Bio-Rad). Pol II fold enrichment was determined by the delta CT method.
310
311 **ChIP-seq library preparation**
312 Libraries for ChIP-seq were prepared with NEBNext Ultra II DNA Library kit (NEB) according to
313 the manufacturer's instructions with the following modifications. Starting DNA for ChIP or input
314 samples was 10 ng. Index primers were from NEBNext Multiplex Oligos for Illumina Dual Index
315 Primer Set 1 and were diluted 1/2.5 before use. Library amplification during indexing
316 amplification was between 6-8 cycles Samples were sequenced (paired-end) on an Illumina
317 NextSeq 2000 P2 flow cell.
318
319 **ChIP-seq analysis**
320 Paired-end raw fastq files were first trimmed for TruSeq3-PE-2 adaptors using Trimmomatic
321 0.38 (41) to remove adaptor readthrough. FastQC was used for quality control analysis.
322 Adapter-trimmed fastq were then aligned to a hybrid genome combining *S. cerevisiae* and *S.*
323 *pombe* genomes using bowtie2/2.4.5 (32), allowing 1 mismatch and disallowing insert size >
324 1000 ('bowtie2 -q -N 1 -X 1000 –x'). The hybrid genome was generated by combining *S.*
325 *cerevisiae* genome version R64-3-1 with *S. pombe* genome 2018-9-4, after appending a suffix
326 of "pom_" to *S. pombe* chromosomes to allow reads mapping to *S. pombe* to be filtered later.
327 Sam files generated from bowtie2 alignment were then converted to bam, which were then
328 sorted and indexed using bamtools. Duplicates were then removed by picard 2.8.12, followed by
329 indexing of newly generated bam files. Subsequent to duplicate removal, reads aligned to hybrid
330 genome were segregated into separate species-specific (*S. cerevisiae* or *S. pombe*) input or IP
331 bam files ('samtools idxstats <non_duplicated-hybrid.bam> | cut -f 1 | grep -v "pom_" | xargs
332 samtools view -b <non_duplicated-hybrid.bam> > <output_S.ce.bam>'; 'samtools idxstats
333 <non_duplicated-hybrid.bam> | cut -f 1 | grep "pom_" | xargs samtools view -b <non_duplicated-
334 hybrid.bam> > <output_pombe.bam>'). Bams were then indexed using samtools/1.14 (33).
335 This segregation of species-specific reads allows counting species specific reads in both input
336 and IP bam files for normalization factor quantification. Total number of unique reads (samtools
337 flag -F 260) per bam file of *S. cerevisiae* and *S. pombe* were counted for both input and IP data
338 for calculating normalization factor combining input and spike-in reads, using an R script. The
339 normalization factor was estimated following method of :
340 (INPUT_Sp_Counts/100000000)/((Sp_Counts/100000000) * (INPUT_Sc_Counts/100000000))
341 (42). These factors were then used to scale the *S.cerevisiae* IP bams to generate scaled or
342 normalized bigwigs using bamCoverage function of deeptools/3.3.0. Wiggletools/1.2.11 (43,44)

was then used to generate mean bedgraphs of three replicates which were then converted to mean bigwigs using bedGraphtoBigWig of kentutils/v.370 (45). Differential bigwigs were generated by log2 operation function of bigwigCompare under the deeptools/3.3.0 package which were then used for generating heatmaps (44).

1H-NMR characterization of Thiolutin reduction and metal binding

Thiolutin stock solution for NMR experiments was freshly prepared by dissolving thiolutin in DMSO-d6. Thiolutin reduction study was performed using freshly prepared DTT in an NMR tube at the final sample concentrations of 1.5mM thiolutin, 7.5mM DTT, 15mM Tris (pH=8.0) and 10% D2O. 1H-NMR spectra were collected immediately using 500MHz Bruker Avance II spectrometer at 25 ˚C. For Zn^{2+} and Mn^{2+} chelation experiments, Zn^{2+} or Mn^{2+} were added at a final concentration of 7.5mM 1 minute after thiolutin reduction by DTT and were incubated at room temperature for 2 minutes before the acquisition of 1H-NMR spectra.

Results

Thiolutin or reduced thiolutin alone fail to inhibit fully purified Pol II in vitro

Recent publications suggest that thiolutin does not directly inhibit Pol II, in contrast to classic in vitro transcription experiments demonstrating thiolutin inhibition of partially purified yeast extract fractions containing Pol I, II, or III (20). We set out to understand this discrepancy by first examining thiolutin inhibition of purified Pol II. Given that thiolutin and holomycin activities could be sensitive to reduction of the disulfide bond by DTT (1,11,12) (Figure 1A), we removed DTT from the in vitro transcription reaction and performed thiolutin treatment with or without molar equivalents of DTT (Figure 1B). Under the buffer conditions employed here, we failed to observe thiolutin inhibition of Pol II, with DTT having no effect (Figure 1B). While these results are consistent with assertions that thiolutin does not directly target Pol II, they might similarly be explained by the absence of a cofactor or subtleties in experimental conditions between *in vitro* assays. We therefore set out to screen for potential co-factors while these biochemical assays are revisited below.

Three independent genetic screens for thiolutin resistant and sensitive mutants

To gain insights into factors controlling the cellular response to thiolutin, we performed three independent genetic screens for modifiers of thiolutin sensitivity (Figure 2A, Figure S1A). First, we performed a conventional forward genetic screen for thiolutin resistant mutants through UV mutagenesis followed by thiolutin resistance selection. The causal mutations for thiolutin resistance were identified by bulk segregant analysis and whole genome sequencing (46) (Figure S1A). Second, we screened a yeast Variomics library for individual thiolutin resistant candidates (31). The Variomics library contained random mutations for almost all yeast genes cloned into a CEN based plasmid and expressed in strains with the relevant endogenous gene deleted. The CEN based plasmid used is known to propagate at 1-2 copies/cell and could result in increased gene dosage (47). Mutants from the forward genetics screen or those reproducibly isolated from the manual Variomics screens were re-tested for resistance (Figure S1B-C, Table S1, S2). Third, we performed a set of high-throughput screens using both pooled Variomics and deletion libraries using barcode-sequencing (Bar-seq) (25,26) (Figure 2A, Material and Methods), where the thiolutin resistant and sensitive mutants were identified by quantifying changes of mutant-linked DNA barcode frequency under thiolutin-treated or control conditions (26,34). Overall, our data exhibited excellent reproducibility (Figure S2) and revealed valuable common and distinct features between Variomics (putative gain-of-function (GOF) and loss-of-function (LOF) mutants combined) and deletion (LOF mutants) libraries (see Material and Methods). We have revealed contribution of multidrug resistance (Figs S1B-E, S3), oxidative stress response (Figs S1F-G, S5), multiple divalent metal homeostasis/trafficking pathways (Figs 2, 3, S7, S8) as well as the proteasome to thiolutin resistance (Fig S6), and we have

394 further genetically dissected a subset of these pathways. These data collectively support that
395 reduction and manganese or other metals appear to contribute to the thiolutin inhibitory activity,
396 supporting a model that reduction and manganese are both required for thiolutin inhibition of Pol
397 II in vitro, tested in subsequent biochemical experiments (Figs 4,5). Each of these pathways is
398 discussed below.
399
400 **Functional dissection of the multidrug resistance (MDR) and oxidative stress response**
401 **(OSR) pathways in response to thiolutin**
402 We identified thiolutin resistant strains harboring mutations in MDR and OSR genes from all
403 three genetic screens. These results are perhaps not surprising given that yeast has well
404 characterized MDR pathways that sense and pump out the toxic small molecules as a self-
405 protection mechanism along with recent reports that thiolutin and holomycin activities require
406 reduction in vitro (11,12). Reduction of thiolutin may itself oxidize cellular proteins and cause
407 oxidative stress. In addition, it has been reported that reduced holomycin may act as a redox
408 cycler, which could possibly generate ROS. Consistent with redox activity, thiolutin appeared to
409 induce expression of several OSR genes (9). However, it has not been examined how thiolutin
410 interacts with either MDR or OSR pathways. In light of our isolated thiolutin resistant mutants,
411 we functionally dissected control of thiolutin sensitivity by these pathways. From both manual
412 Variomics and forward genetic screens, we isolated multiple mutants in *YAP1* and *YRR1*,
413 encoding transcription factors that have been implicated in OSR and/or MDR, respectively
414 (Figure S1C). In addition, we also isolated mutants in the MDR efflux pump gene *SNQ2* from
415 the manual Variomics screen. Finally, from high-throughput Bar-seq screens, we identified
416 distinct thiolutin resistance and sensitivity in additional mutants linked to MDR transcription
417 factors or efflux pumps (Figure 2B). Several lines of evidence suggested that the isolated
418 thiolutin resistant MDR mutants were GOF mutations. First, isolated *yap1* mutations were
419 clustered in C-terminal regions, where a variety of mutants are known to cause GOF (48-52).
420 Second, isolated MDR mutants from the manual Variomics screen were dominant or functioned
421 through increased dosage (overexpression) (Figure S3). Third, in Bar-seq screens, we found
422 Variomics mutants in several MDR genes (*YAP1, YRR1, SNQ2*) conferred thiolutin resistance
423 whereas deletion of the same genes either conferred sensitivity or had no strong effect (Figure
424 2B), consistent with these MDR Variomics mutants being different from the gene deletion
425 mutants (complete LOF).
426
427 To determine the nature of identified MDR mutants from our screens, we constructed a series of
428 MDR gene deletion mutants and tested their sensitivity to thiolutin (Figure S1D). We found that
429 none of the tested deletion mutants was thiolutin resistant (Figure S1D). The lack of resistance
430 for all the tested MDR deletion strains is consistent with the isolated thiolutin resistant MDR
431 mutants from Variomics and forward genetics screens increasing MDR activity. In addition,
432 *pdr1*Δ and *snq2*Δ conferred hypersensitivity to thiolutin (Figure S1D), consistent with the Pdr1
433 and Snq2 functions in promoting thiolutin resistance for WT strains. Together, we conclude that
434 the MDR transcription factor Pdr1 is the major transcription factor promoting efflux of thiolutin
435 from the cell, whereas neither Yrr1 nor Yap1 appeared to promote baseline resistance, given
436 that *yap1*Δ and *yrr1*Δ did not confer thiolutin hypersensitivity. However, increased Yap1 or Yrr1
437 activities through mutations or dosage may increase efflux pump expression to promote thiolutin
438 resistance, through their known linkage to many multidrug efflux pumps (53-55).
439
440 Holomycin did not inhibit yeast cell growth at low concentration (22), and we recapitulated these
441 observations (Figure S4A). Given that structurally similar compounds may have different cell
442 permeability and efflux efficiency, we asked whether the same set of MDR deletion strains
443 conferred sensitivity to holomycin, but failed to observe any (Figure S4A). This observation
444 suggested that the lack of holomycin sensitivity may not be due to selective efficiency of drug

445 efflux, although we cannot rule out the possibility that thiolutin and holomycin may be
446 transported by different efflux pumps.
447
448 In addition to MDR pathways, we also identified thiolutin-modulating mutations in OSR-related
449 genes, including *YAP1* (discussed above) and genes in the thioredoxin pathway. Thioredoxins
450 are a series of small anti-oxidant proteins that primarily function in reducing specific cysteines in
451 client proteins (reviewed in (56) and references therein), and in turn are themselves reduced by
452 thioredoxin reductases (Figure S1F). In yeast, there are two thioredoxin reductases
453 (cytoplasmic Trr1 and mitochondrial Trr2) and three thioredoxins (cytoplasmic Trx1, Trx2;
454 mitochondrial Trx3) (Figure S1F). Mutants in *TRR1* were reproducibly isolated from our manual
455 Variomics screen (Figure S1B,E; Table S1). In addition, *TRR1** and *TRX1** plasmid bearing
456 strains obtained from from high-throughput screening of Variomics libraries were resistant to
457 thiolutin but not *trr1*Δ or *trx1*Δ were not (Figures 2B), suggesting that *TRR1** and *TRX1**
458 plasmids in the Variomics library could be GOF due to specific mutation or increased dosage of
459 the plasmid.
460
461 *TRR1* was found to be essential in large scale gene deletion analysis (57) but nonessential in
462 classical genetic experiments (58-62). To understand the nature of *TRR1* function in thiolutin
463 resistance/sensitivity, we constructed a *trr1*Δ strain to directly test its thiolutin sensitivity (Figure
464 S1G). Interestingly, *trr1*Δ conferred hypersensitivity to thiolutin (Figure S1G), consistent with
465 Trr1 activity antagonizing thiolutin and specific *TRR1** mutants or increased Trr1 dosage
466 enhancing this antagonism. The Trr1 function in antagonizing thiolutin also suggests that our
467 isolated *yap1* alleles could confer thiolutin resistance through promoting *TRR1* expression,
468 among other mechanisms.
469
470 We conceive of *trr1*Δ hypersensitivity to thiolutin in two ways. It could be due to loss of Trr1
471 function in directly counteracting thiolutin activity or the accumulation of oxidized thioredoxins, or
472 both. The observed *TRX1**-linked thiolutin resistance in high-throughput Variomics screens
473 suggested critical functions of thioredoxin(s) in thiolutin resistance downstream of *TRR1*.
474 Therefore, we examined thioredoxin deletions directly for thiolutin resistance. We found that the
475 *trx1*Δ, *trx2*Δ, or *trx1*Δ *trx2*Δ mutants did not confer thiolutin sensitivity (Figure S1G). In contrast,
476 *trx1*Δ *trx2*Δ conferred thiolutin resistance, and further, suppressed thiolutin hypersensitivity of
477 *trr1*Δ (Figure S1G), consistent with the hypothesis that *trr1*Δ hypersensitivity to thiolutin is due to
478 accumulation of oxidized thioredoxins. The observed *trx1*Δ *trx2*Δ thiolutin resistance reveals
479 critical requirement of Trx1 and Trx2 for thiolutin activity *in vivo* and suggests that Trx1 and Trx2
480 may function either directly or indirectly in thiolutin reduction. However, further experiments are
481 needed to test the direct thiolutin reduction by Trx1 or Trx2.
482
483 Thiolutin resistance conferred by *yap1* alleles and thioredoxin mutants suggests possible
484 connections to OSR. Therefore, we set to test the roles of two additional OSR genes, *TSA1*,
485 encoding a thioredoxin peroxidase, and *SOD1*, encoding a cytosolic copper-zinc superoxide
486 dismutase, in thiolutin resistance. Interestingly, *sod1*Δ, but not *tsa1*Δ, conferred hypersensitivity
487 to thiolutin (Figure S1G). Given that holomycin is a known redox cycler, we asked if simple
488 addition of H_2O_2 could mimic the thiolutin effect in tested thioredoxin and OSR gene deletion
489 mutants (Figure S1G). Thiolutin sensitivities in tested strains were distinct from H_2O_2
490 sensitivities, suggesting distinct effects on cellular function. Finally, we tested if yeast could be
491 sensitized to holomycin by the same set of mutants (Figure S4). Interestingly, *trr1*Δ and *sod1*Δ
492 were slightly sensitive to 10 µg/mL holomycin (Figure S4), suggesting that the induction of
493 oxidative stress could be general property of dithiolopyrrolone compounds and that yeast are at
494 least somewhat permeable to holomycin.
495

496 **Thiolutin induces apparent oxidative stress**
497 Multiple lines of evidence presented above indicated that thiolutin may induce oxidative stress
498 and increased Yap1 function may promote thiolutin resistance. Yap1 functions by sensing the
499 cellular oxidants through its C-terminal cysteines, causing it to translocate into the nucleus and
500 up-regulating a series of OSR genes to counteract the cellular oxidants upon oxidative stress
501 (48-52). Therefore, nuclear localization of Yap1 is in general a sign of increased Yap1 function
502 and OSR (48,51,52). To test whether thiolutin treatment caused nuclear translocation of Yap1,
503 we fused *YAP1* to sequence encoding EGFP on the Yap1 C-terminus, and monitored
504 Yap1::EGFP localization after thiolutin treatment. Thiolutin indeed induced Yap1::EGFP nuclear
505 localization, consistent with induction of oxidative stress, although the thiolutin-induced
506 Yap1::EGFP nuclear translocation appeared to be slower and weaker than that induced by H_2O_2
507 (Figure S5). In addition, thiolutin depleted total glutathione within an hour of treatment (Figure
508 S6A). However, thiolutin depleted both active GSH and GSSG, a behavior similar to glutathione
509 synthesis defective mutants but distinct from several well-known oxidants such as H_2O_2 and
510 menadione (63-65). In contrast, holomycin effect weak at best on Yap1 localization and did not
511 affect cellular glutathione levels (Figure S6A), consistent with the lack of growth inhibition by
512 holomycin and distinct activities or trafficking in yeast between the two structurally similar
513 compounds.
514
515 Previous studies suggested that the reduced holomycin was spontaneously re-oxidized when
516 exposed to air (1), consistent with the behavior of redox-cycling compounds. To test if thiolutin
517 exhibited similar behavior, we monitored thiolutin reduction and re-oxidation by its unique UV
518 absorbance due to the conjugated ene-dithiol groups (Figure S6B, C), as with the recent reports
519 (1,11,12). Thiolutin could be reduced by DTT or TCEP, but not equimolar glutathione (Figure
520 S6B), consistent with the behavior of holomycin (1). Reduced thiolutin could be also re-oxidized
521 (Figure S6C), suggesting that thiolutin can act as a redox-cycler, similar to holomycin (1).
522 Together, thiolutin induced the Yap1 nuclear accumulation and hypersensitivity of *sod1*Δ and
523 *trr1*Δ mutant in vivo and appeared to be a redox cycler in vitro, consistent with the induction of
524 oxidative stress.
525
526 DNA damage can be a consequence of redox-cycling and can lead to transcription inhibition
527 and cytotoxicity (66,67). We asked if thiolutin treatment could cause DNA damage or decrease
528 viability. We did not observe an increase in mutation rate as measured by resistance to
529 canavanine, consistent with little or no effect on DNA damage rates, nor did we observe a
530 viability defect over the period of treatment (Figure S6D, E). The lack of viability defect is
531 consistent with an early report showing that thiolutin inhibition was reversible after several
532 hours' treatment (68). Together, we suggest that thiolutin is a redox cycler in vitro and possibly
533 also in vivo but does not appear to inhibit transcription through widespread DNA damage.
534
535 **Additional cellular pathways are involved in thiolutin resistance**
536 The high-throughput screens of pooled yeast Variomics and deletion libraries, compared to
537 conventional forward genetics and manual Variomics screens, revealed several additional
538 pathways in thiolutin resistance (Figure 2B). We isolated mutants involved in metal
539 homeostasis, SWI/SNF complex, proteasome, ribosomal RNA biogenesis, and small ribosomal
540 subunits (Figure 2B). Many observations from the Variomics screens were already
541 independently confirmed from two conventional screens, direct deletion analyses, or the existing
542 literature (Figure S1, Table S2). For example, deletion of SWI/SNF complex subunits *SWI3* and
543 *SNF12* have been shown to confer sensitivity to a variety of divalent metals including Mn^{2+},
544 Zn^{2+}, Co^{2+} and Cd^{2+} (69-73), consistent with thiolutin perturbation of metal homeostasis
545 (discussed more below). We further constructed 9 haploid (for non-essential genes) or
546 heterozygous (for essential genes) deletion mutants to validate the observation from the bar-seq

547 screens of the deletion libraries. We validated the observations in 7 out of 9 mutants, including
548 one resistant and one sensitive mutant from the non-essential deletion pool, and 5 resistant
549 mutants from essential heterozygous diploid pool (Figure S7). Among them, we validated the
550 observed thiolutin resistance conferred by three strains heterozygous for deletions in
551 proteasome subunit genes (*PRE10/pre10*Δ, *PUP1/pup1*Δ, *RPN5/rpn5*Δ) (Figure S7).
552
553 The reconstructed strains validated the surprising but clear observation that heterozygous
554 deletion mutants in proteasome subunit genes universally conferred thiolutin resistance (Figure
555 S7). This is surprising because thiolutin was recently demonstrated to be a proteasome inhibitor
556 through Zn^{2+} chelation, and heterozygous proteasome subunit deletion mutants presumably
557 may lead to reduced proteasome activity and would be expected to confer sensitivity to
558 proteasome inhibitors. Interestingly, two recent reports observed similar paradoxical resistance
559 to proteasome inhibitors in yeast strains and human cell lines with decreased level of the
560 regulatory 19S proteasome subunits (74,75). In yeast and human, the fully assembled 26S
561 proteasome consists of a 20S catalytic core and a 19S regulatory complex. It was demonstrated
562 that decrease or transient inhibition of 19S proteasome subunits may in turn induce the level
563 and activity of partially assembled 20S proteasome instead of the fully assembled 26S
564 proteasome (75), resulting in a net increase of proteasome function. It was also recently
565 suggested that specific reduced expression of 19S proteasome subunits induced an altered
566 cellular state and altered the global transcriptome in response to proteasome inhibitors (76).
567 However, our observation is distinct, because we observed decreases in both 19S and 20S
568 proteasome subunits conferred thiolutin resistance. Whether the proteasome has increased
569 level and activity in these strains has yet to be tested.
570
571 **Thiolutin alters divalent metal homeostasis**
572 The recent detection of direct Zn^{2+} chelation activity of reduced thiolutin and holomycin explains
573 multiple thiolutin-induced phenotypes, such as inhibition of proteasome and glucose metabolism
574 (8,11,12). From the high-throughput screens, we observed distinct thiolutin resistance or
575 sensitivity linked to diverse Zn^{2+} trafficking genes, including those encoding the master
576 transcription regulator Zap1 and various Zn^{2+} transporters Zrt1, Zrt2, Zrc1 and Cot1 (Figure 2B).
577 Variomics strains linked to *ZAP1, ZRT1, ZRT2, ZRC1* and *COT1* conferred thiolutin resistance
578 whereas deletion mutants were either not resistant (*zrt1*Δ, *zrc1*Δ, *cot1*Δ) or hypersensitive
579 (*zap1*Δ and *zrt2*Δ) (Figure 2B), suggesting that these Variomics mutants could be gain-of-
580 function or dosage modifiers of thiolutin resistance.
581
582 We first constructed a *zap1*Δ strain and tested its sensitivity to thiolutin (Figure 3A). *zap1*Δ
583 confers hypersensitivity to thiolutin, consistent with Zap1 function in cellular resistance to
584 thiolutin and thiolutin alteration of Zn^{2+} homeostasis *in vivo*. Notably, *zap1*Δ also conferred
585 hypersensitivity to holomycin (Figure S8A). This observation is consistent with the reports that
586 altering zinc homeostasis is a conserved mechanism among dithiolopyrrolones, and that
587 holomycin could deplete cellular Zn^{2+} or access other essential targets in yeast if zinc
588 homeostasis were otherwise perturbed, and suggesting that yeast resistance to holomycin may
589 be partially explained by efficient transportation of Zn^{2+} that counteracts holomycin. *zap1*Δ
590 hyper-sensitivity to thiolutin and holomycin was much stronger than that to H2O2, suggesting
591 the *zap1*Δ hypersensitivity to thiolutin and holomycin were distinct from general oxidative stress
592 exacerbation by zinc deficiency (77-80). and likely to Zn^{2+} homeostasis defects. Finally, Zn^{2+}
593 supplementation at high concentration partially suppressed thiolutin inhibition (Figure S8C). The
594 lack of full suppression suggests that there may be other thiolutin-mediated defects in addition
595 to Zn^{2+} chelation, although we cannot rule out that inefficient Zn^{2+} trafficking limits effective Zn^{2+}
596 supplementation in the cell.
597

598 In addition to Zn^{2+} homeostasis mutants, we observed genes involved in Mn^{2+} trafficking (*PMR1,*
599 *CCC2, VPS17, VPS25, SMF2*) linked to thiolutin resistance (Figure 2B). Interestingly, *PMR1* is
600 a high affinity Ca^{2+} and Mn^{2+} ATPase that is required for Ca^{2+} and Mn^{2+} transport to Golgi and
601 subsequent export (81,82). *pmr1*Δ has been shown to increase intracellular Mn^{2+} level and
602 appeared to confer thiolutin sensitivity (Figure 2B), which we confirmed by reconstructing *pmr1*Δ
603 mutant and plate phenotyping (Figure 3B, Figure S9A). In contrast, deletion of *SMF2*, a
604 transporter for importing divalent metals including Mn^{2+}, has been shown to cause intracellular
605 Mn^{2+} depletion and conferred slight but consistent thiolutin resistance (Figure S8A). Together,
606 the intracellular level of Mn^{2+} appeared to be positively correlated with thiolutin hypersensitivity,
607 suggesting a mechanism distinct from Zn^{2+}, where Zn^{2+} supplementation confers partial thiolutin
608 resistance (Figure S8C). To rule out the possibility that this altered thiolutin sensitivity is due to
609 indirect effect from interference of other divalent metals, we phenotyped wild-type yeast strain in
610 the presence of thiolutin and Mn^{2+} supplementation. Indeed, we observed that Mn^{2+} dose
611 dependently exacerbated thiolutin sensitivity in wild-type yeast, supporting the synergy between
612 Mn^{2+} and thiolutin *in vivo* (Figure 3C).
613
614 In addition to *pmr1*Δ, we also confirmed the thiolutin hypersensitivity of *vps17*Δ and *vps25*Δ
615 (Figure S9A). Vps17 and Vps25 are two vacuolar protein sorting genes and have been
616 implicated in degradation of the Mn^{2+}-importing protein Smf1, thus possibly causing intracellular
617 accumulation of Mn^{2+} and conferring thiolutin hypersensitivity. However, *vps17*Δ and *vps25*Δ
618 were not more sensitive to Mn^{2+} than WT in our strain background (Figure S9B) and we found
619 that *smf1*Δ did not suppress the hypersensitivity conferred by *vps17*Δ or *vps25*Δ (Figure S9A),
620 suggesting that other mechanisms may be involved in these two Vps mutants.
621
622 Given the contrasting Zn^{2+} and apparent Mn^{2+} modulation of thiolutin activity, and that metal
623 homeostasis is complex with cross-talk between metals, we examined the intersection between
624 divalent cations (Cd^{2+}, Co^{2+}, Cu^{2+}, and Mg^{2+} to compare with Mn^{2+}), thiolutin, and thiolutin-
625 sensitive deletions (*zap1*Δ, *pmr1*Δ, and *sod1*Δ). We also compared thiolutin with 1,10-
626 phenanthroline (1,10-pt), a chemically distinct Zn^{2+} chelator that can inhibit yeast transcription *in*
627 *vivo* (83-85) (Figure 3D). Co^{2+}, Cu^{2+}, and Mn^{2+} sensitized yeast to thiolutin specifically but not to
628 1,10-pt. The tested deletion strains appeared more sensitive to thiolutin than to 1,10-pt at the
629 concentrations tested. 1,10-pt sensitivity was highest for *zap1*Δ, consistent with 1,10-pt function
630 as a Zn^{2+} chelator. We also observed distinct effects of different 1,10-pt levels and suppression
631 of *sod1*Δ sensitivity to 40 μM 1,10-pt by Cu^{2+} and Mn^{2+}. These results suggest that thiolutin and
632 1,10-pt are distinct, especially in relationships to metals other than Zn^{2+}.
633
634 We tested whether reduced thiolutin chelates Mn^{2+} and Cu^{2+}, while also confirming Zn^{2+}
635 chelation. Consistent with two recent reports (11,12), Zn^{2+} caused a distinct UV shift of reduced
636 thiolutin from ~340nm to ~370nm but did not change the UV spectra of non-reduced thiolutin
637 (Figure 3E, Figure S9C). In addition, we found that Mn^{2+} and Cu^{2+} can also interact with reduced
638 but not non-reduced thiolutin, in a manner likely similar to Zn^{2+} binding (Figure 3E). Consistently,
639 1H-NMR experiments confirmed that DTT caused chemical shifts consistent with reduction of
640 the ene-disulfide in thiolutin, and further chemical shifts caused by diamagnetic Zn^{2+} and
641 selective broadening caused by paramagnetic Mn^{2+} were consistent with interactions between
642 the divalent metals and the thiolutin sulfhydryls (Figure S9, D and E). In contrast, Mg^{2+} did not
643 bind to reduced thiolutin, distinct from the other tested metals (Figure 3E).
644
645 **Thiolutin, when activated by DTT and Mn^{2+}, directly inhibits Pol II in vitro**
646 Despite the progress in understanding thiolutin induced cellular phenotypes, whether and how
647 thiolutin directly inhibits yeast Pol II *in vitro* remained unresolved. Multiple lines of evidence
648 suggest possible involvement of divalent metals in this process. First, the co-clustering of

649 thiolutin and bathophenanthroline induced phenotypic profiles suggests similar modes of action
650 (Figure 2C). Bathophenanthroline is highly similar to 1,10-pt (Figure S10), which was suggested
651 to require Cu^{2+} for direct transcription inhibition in vitro (28,86), though these compounds may
652 have similar activities because they are also well-known Zn^{2+} chelators (87). Second, the direct
653 interaction between reduced thiolutin and divalent metals (Zn^{2+}, Mn^{2+} or Cu^{2+}) suggests the
654 possibility that thiolutin may function with multiple metal co-factors.
655
656 Many divalent metals inhibit RNAP activity (e.g. Pb^{2+}, Zn^{2+}, Cu^{2+}, Be^{2+}, Cd^{2+}, Ca^{2+}) (88), and
657 additionally are tightly controlled in cells due to toxicity (*e.g.* Fe^{2+}, Co^{2+}), so may not participate
658 in possible Pol II inhibition by thiolutin. Mn^{2+} does not inhibit RNAP but instead increases the
659 activity of multiple RNA polymerases (including Pol II) (88). In addition, Mn^{2+} is readily available
660 in yeast cells (0.04-2mM depending on the type of measurement while genetically shown to be
661 at levels that likely can alter Pol II activity *in vivo*) (89-93) at a relevant range to the reported
662 thiolutin inhibitory concentration (~20μM in (20)). We note that in the original Tipper
663 observations (20), their transcription buffer contained 1.6 mM Mn^{2+} as many classical
664 transcription buffers included both Mn^{2+} and Mg^{2+} to maximize observed activity. In contrast,
665 most other studies did not report Mn^{2+} in buffers (12,18,21,22) (One report appears to have a
666 high concentration Mn^{2+} (10 mM) and possibly also reductant (19)). Therefore, we set out to test
667 whether Mn^{2+} might participate in thiolutin-mediated inhibition of Pol II. Remarkably, Mn^{2+}
668 addition to reduced thiolutin potently inhibited purified Pol II activity (Figure 4A), in sharp
669 contrast to the activation of Pol II activity caused by Mn^{2+} by itself in the absence of reduced
670 thiolutin. Our observation is consistent with the known stimulation of RNAPs by Mn^{2+} (88,94), but
671 also suggests a potent Pol II inhibition by Mn^{2+} activated reduced thiolutin (hereafter termed as
672 Thio/Mn^{2+}) (Figure 4A, Quantification of thiolutin treatments and controls in Figure 4C,D).
673
674 We next designed a series of experiments to investigate properties of the inhibited Pol II and
675 nature of the inhibitory species. We first tested if order-of-addition among Pol II, DNA and
676 Thio/Mn^{2+} was critical for the inhibition, since order-of-addition is often informative on the mode
677 of transcription inhibition (Figure 4B, E). This is especially important given the observation of
678 Tipper that order-of-addition was critical for thiolutin inhibition in that study (20). Consistent with
679 the early observation, we found that the template binding protects Pol II from the Thio/Mn^{2+}
680 inhibition (Figure 4B). Template protection of Pol II suggests Thio/Mn^{2+} inhibits Pol II DNA
681 interaction or similarly early step in transcription, consistent with the behavior of transcription
682 initiation inhibitor. Therefore, we tested if Thio/Mn^{2+} affected Pol II elongation on a transcription
683 bubble template using an RNA primer, where transcription initiation is bypassed (Figure 4E).
684 Surprisingly, Thio/Mn^{2+} altered, but did not block Pol II transcription elongation, inducing a highly
685 pause prone Pol II elongation mode (Figure 4E). This was unexpected because most specific
686 initiation inhibitors do not cause elongation defects, and DNA binding does not protect RNAPs
687 from elongation inhibitors by their very nature. In addition, pre-assembled transcription
688 elongation complexes were also resistant to Thio/Mn^{2+} (Figure 4E, bottom middle panel),
689 validating the critical order-of-addition in the non-specific transcription assay (Figure 4B).
690 Thio/Mn^{2+} inhibited Pol II was pause-prone and appeared to irreversibly arrest at specific
691 template positions (Figure 4E, bottom right panel).
692
693 Whether thiolutin inhibits transcription initiation or elongation *in vivo* is unclear (17,21). In light of
694 our *in vitro* results, we tested thiolutin mediated Pol II transcription inhibition *in vivo*, first by
695 monitoring Pol II occupancy on a long gene, *YLR454W* driven by the *TEF1* promoter, and then
696 by Pol II ChIP-seq genome wide (Figure 5). We observed a specific decrease of Pol II
697 occupancy by qPCR on the 5′ end of *YLR454W* within the first 2 minutes of thiolutin treatment,
698 consistent with fast transcription initiation inhibition after thiolutin treatment (Figure 5). After 2
699 minutes, we also observed a relatively slower loss of Pol II from the template compared to

700 previous experiments where transcription initiation was inhibited by other means, specifically by
701 glucose shutoff or by carbon starvation of transcription from a *GAL1* promoter driven *YLR454W*
702 reporter (37). Additionally, this decrease in Pol II occupancy at later time points does not fully
703 cover the 3′ end endas it does at *GAL1p::YLR454W* under the aforementioned inhibition
704 conditions where the gene is clear of Pol II by 4-6 minutes (37). These results suggest that
705 thiolutin may have additional non-immediate inhibitory effects on Pol II elongation *in vivo* and
706 that thiolutin treatment is not functioning solely through altering cellular signaling (*e.g.* through
707 inhibition of the Tor pathway (7)) (Figure 5A). To assess kinetics of effects on Pol II occupancy
708 in response to thiolutin treatment genome wide, we performed ChIP-seq for a FLAG-tagged
709 Rpb3 Pol II component in triplicate upon thiolutin treatment (1, 2, 4, 8 minutes), DMSO vehicle
710 treatment (8 minutes), or control cells (Figure 5B-D, Figure S11). Our ChIP-seq protocol
711 includes spike-in of Rpb3-FLAG chromatin from *S. pombe* allowing for determination of global
712 effects (Figure 5B). Our experiments showed good reproducibility across replicates (Figure
713 S11A,B)) with a clear trend of increased effects over time of thiolutin inhibition. We find
714 evidence of broad decrease in Pol II occupancy genome wide (Figure 5C). We observe a
715 continuum of effects for highly expressed genes where ribosomal protein (RP) genes are
716 affected more strongly, then ribosome biogenesis genes (RiBi), then other genes (Figure 5D,
717 5E). These results are consistent with reported inhibition of the Tor pathway upon thiolutin
718 treatment but also more widespread decreases in Pol II occupancy. Consistent with our
719 observation at *TEF1p::YLR454W*, metaplots for all genes in the top 40% of Pol II occupancy
720 ≥1.5kb in length show an initial decrease in Pol II occupancy at the 5′ end upon thiolutin
721 treatment (Figure S11C). These results are consistent with thiolutin inhibition of Pol II initiation
722 but with additional effects on elongation both *in vitro* and *in vivo*.
723
724 To investigate the nature of the inhibitory species, we further examined thiolutin interaction with
725 Mn^{2+}. Interestingly, we observed continuous and reproducible changes of the UV spectra after
726 Mn^{2+} was added to reduced thiolutin (Figure 6A), suggesting changing chemical species in the
727 reaction. The peak of UV absorbance was shifted from 340nm (reduced thiolutin) to around
728 380nm in the first two minutes, with subsequent decrease in the 380nm peak as a third species
729 at 300nm started to accumulate (Figure 6A). The reaction reached a relative stable equilibrium
730 after 20 minutes. Our data revealed the dynamic change and two major species after Mn^{2+}
731 addition to the reduced thiolutin but could not distinguish how either of these related to the
732 inhibitory species. To test this question, we prepared Thio/Mn^{2+} and either freshly treated Pol II
733 or incubated at room temperature for 20 minutes before treating Pol II (Figure 6B). Remarkably,
734 we observed strong Pol II inhibition by freshly prepared Thio/Mn^{2+} but complete loss of
735 Thio/Mn^{2+} inhibitory activity after 20 minutes (Figure 6B). This result is consistent with the
736 380nm species possibly contributing to Pol II inhibition yet being unstable in solution. In contrast
737 to the window for inhibitory activity of Thio/Mn^{2+}, immediately treated Pol II was inhibited for up
738 to 50 minutes (20-minute incubation and 30-minute reaction time), suggesting that the Pol II
739 inhibition was stable (Figure 6B).
740
741 We propose two models to reconcile the observation that Pol II stabilized the unstable 380nm
742 inhibitory species. First, Pol II might stabilize the inhibitory species in a tight pocket that
743 prevented further reaction into other inactive species. Second, Mn^{2+} might coordinate with
744 reduced thiolutin to form a disulfide bond within Pol II or possibly a thiolutin adduct, as Cu^{2+}
745 does to facilitate disulfide formation through cysteine sulfenylation in other proteins (95-97). If
746 sulfenylation and disulfide bond formation were involved, the Thio/Mn^{2+} inhibition is expected to
747 be suppressible by a high concentration of DTT. Indeed, we found that excess DTT abolished
748 the inhibition, consistent with the involvement of reductant sensitive inhibition (Figure 6C).
749
750 **Discussion**

751 Thiolutin is a well-known transcription inhibitor that has been used in mRNA stability studies, but
752 its mode of inhibition has been complicated and unresolved. It has been demonstrated that
753 reduced thiolutin and the related natural product holomycin chelate Zn^{2+} in vitro, and thiolutin
754 chelation of Zn^{2+} could specifically inhibit diverse classes of metalloproteins (11,12). However,
755 these previous reports tested failed to observe direct thiolutin inhibition of RNAPs, under
756 conditions where Zn^{2+} chelation was permissible. Here we present three independent genetic
757 screens for thiolutin resistant or sensitive mutants, providing a genetic basis for understanding
758 thiolutin-altered cellular responses and reveal a direct mode of action against Pol II *in vivo*. We
759 show that alterations in diverse cellular pathways can modulate cellular sensitivity to thiolutin. In
760 light of our genetic results, we discovered that both reductant DTT and Mn^{2+} together activate
761 thiolutin for direct inhibition of Pol II function, countering the recent narrative while confirming
762 classic observations (11,20).
763
764 **Thiolutin inhibits Pol II through a novel mode of action**
765 We propose that Thio/Mn^{2+} inhibits Pol II through a novel mode of action. The critical order of
766 treating Pol II with thiolutin prior to template DNA binding is a stereotypical behavior for RNAP
767 clamp inhibitors (23,24,98-101), which are distinct from inhibitors targeting the active site, NTP
768 uptake, or RNA exit channels. In addition, we show that thiolutin inhibits Pol II elongation on an
769 initiation-bypassing transcription bubble template, distinct from all the three characterized *E. coli*
770 RNAP inhibitors that lock the clamp in the closed state (Myxopronin (Myx), Corallopyronin (Cor),
771 and Ripostatin (Rip)) that do not inhibit RNAP elongation (23,102). It should be noted that
772 Lipiarmycin (Lpm), an inhibitor that appears to lock the clamp in the partially or fully open state
773 (24), has never been tested on a bubble template. Therefore, thiolutin behaves differently from
774 Myx, Cor and Rip, but further experiments are in need to test whether thiolutin behaves similarly
775 to Lpm. Finally, the exact thiolutin binding site on Pol II remains unclear, and our data cannot
776 rule out the possibility that thiolutin may inhibit Pol II regions other than clamp-controlling switch
777 regions.
778
779 **Diverse cellular pathways modulate thiolutin multiple modes of action**
780 Our genetic screens reveal the contribution of diverse cellular pathways in thiolutin sensitivity.
781 Many of these pathways can be reconciled in a unified model based on current understanding of
782 thiolutin mode of action. In the cell, the thiolutin intra-molecular disulfide bond appears to be
783 reduced, and we propose thioredoxins Trx1 and Trx2 directly or indirectly contribute to thiolutin
784 reduction (along with glutathione) or are responsive to thiolutin oxidation of other proteins,
785 thereby promoting thioredoxin oxidation. Reduced thiolutin subsequently chelates Zn^{2+} to inhibit
786 multiple metalloproteins (*e.g.* Rpn11 and conferring block to proteasomal degradation of
787 substrates), affects Zn^{2+} homeostasis, interacts with Mn^{2+} to inhibit Pol II transcription (and
788 possibly Pol I and III), or become re-oxidized by molecular oxygen. Mn^{2+}, Co^{2+}, and Cu^{2+} also
789 sensitize cells to thiolutin treatment while 1,10-pt does not, suggesting these interactions may
790 not be caused by Zn^{2+} starvation. The reduction or redox cycling of thiolutin may induce the
791 observed Yap1 nuclear localization and oxidative stresses. In addition, we have shown that
792 reduced thiolutin may also chelate other divalent metals such as Cu^{2+} (but not Mg^{2+}), but
793 whether other thiolutin-metal complexes have additional activities remain to be further tested.
794
795 **Thiolutin should be used as a tool with caution**
796 Our work underpins the caveats for using thiolutin to investigate other cellular processes, as
797 suggested by previous studies (10-12). As a routinely used transcription inhibitor to study mRNA
798 stability, it was shown that thiolutin itself inhibits mRNA degradation and complicates the
799 quantitation of mRNA half-life at higher doses (10). Our work here and prior work discussed
800 above suggest that thiolutin is multifunctional and has pleiotropic effects.
801

802 **Thiolutin mode of action may reveal insights into Pol II pausing**
803 The thiolutin induced pause (and arrest) pattern appears to be highly specific and position-
804 dependent, and it will be interesting to further investigate the pause sequence preference and
805 its possible connection to a specific inhibited Pol II conformation. As discussed above,
806 biochemical properties of thiolutin inhibited Pol II most closely resembles clamp inhibition by a
807 locked non-closed state, possibly a partially or fully open state. It is tempting to hypothesize that
808 the thiolutin-induced pause prone Pol II is linked to a specific Pol II conformation. This
809 hypothesis is also consistent with the observations in *E. coli* RNAP that paused elongation
810 complexes appear to correlate with open clamp and TL states, which can be reversed and
811 possibly regulated by elongation factor RfaH (103,104). It has been proposed that this RfaH (a
812 homolog of Spt5 in eukaryotes) pause suppression through the RNAP clamp may be a
813 conserved regulatory mechanism for RNAP elongation in all domains of life (105). Further
814 characterization of thiolutin inhibited Pol II may reveal additional insights into this process in
815 eukaryotes.
816
817 **Acknowledgements**
818 We thank Xuewen Pan for the kind gift of Variomics libraries, and Guillermo Calero for one of
819 the Pol II purifications used here. We thank Alex Francette and Karen Arndt for the gift of *S.*
820 *pombe* chromatin and for advice and sharing of scripts for ChIP-seq analyses. We thank Allyson
821 O'Donnell for advice on analysis of *YAP1-GFP* imaging and data analysis. We acknowledge
822 funding from NIH R01GM097260 and R35GM144116 to CDK and also Welch Foundation Grant
823 A-1763 to CDK for support on this project while our lab was at Texas A&M University. We
824 acknowledge NSF for funding a Research Experience for Undergraduates site grant DBI-
825 0851611 to Texas A&M Department of Biochemistry and Biophysics for support of AJL, SU, and
826 EMP.
827
828 **Data availability**
829 Sequencing data are available in the Sequence Read Archive and are compiled under
830 Bioproject PRJNA725683. Similarly, processed data for ChIP-seq have been deposited in GEO
831 and can be accessed through Bioproject PRJNA725683. Scripts for data analysis are found at
832 https://github.com/Kaplan-Lab-Pitt/Thiolutin.
833
834

References

1. Li, B. and Walsh, C.T. (2011) Streptomyces clavuligerus HlmI is an intramolecular disulfide-forming dithiol oxidase in holomycin biosynthesis. *Biochemistry*, **50**, 4615-4622.
2. Li, B., Wever, W.J., Walsh, C.T. and Bowers, A.A. (2014) Dithiolopyrrolones: biosynthesis, synthesis, and activity of a unique class of disulfide-containing antibiotics. *Natural product reports*, **31**, 905-923.
3. Rossini, C., Taylor, W., Fagan, T. and Hastings, J.W. (2003) Lifetimes of mRNAs for clock-regulated proteins in a dinoflagellate. *Chronobiol Int*, **20**, 963-976.
4. Grigull, J., Mnaimneh, S., Pootoolal, J., Robinson, M.D. and Hughes, T.R. (2004) Genome-wide analysis of mRNA stability using transcription inhibitors and microarrays reveals posttranscriptional control of ribosome biogenesis factors. *Molecular and cellular biology*, **24**, 5534-5547.
5. Kebaara, B.W., Nielsen, L.E., Nickerson, K.W. and Atkin, A.L. (2006) Determination of mRNA half-lives in Candida albicans using thiolutin as a transcription inhibitor. *Genome*, **49**, 894-899.
6. Morey, J.S. and Van Dolah, F.M. (2013) Global analysis of mRNA half-lives and de novo transcription in a dinoflagellate, Karenia brevis. *PLoS One*, **8**, e66347.
7. Eshleman, N., Luo, X., Capaldi, A. and Buchan, J.R. (2020) Alterations of signaling pathways in response to chemical perturbations used to measure mRNA decay rates in yeast. *Rna*, **26**, 10-18.
8. Bergmann, R. (1989) Thiolutin inhibits utilization of glucose and other carbon sources in cells of Escherichia coli. *Antonie Van Leeuwenhoek*, **55**, 143-152.
9. Monje-Casas, F., Michan, C. and Pueyo, C. (2004) Absolute transcript levels of thioredoxin- and glutathione-dependent redox systems in Saccharomyces cerevisiae: response to stress and modulation with growth. *Biochem J*, **383**, 139-147.
10. Pelechano, V. and Perez-Ortin, J.E. (2008) The transcriptional inhibitor thiolutin blocks mRNA degradation in yeast. *Yeast*, **25**, 85-92.
11. Lauinger, L., Li, J., Shostak, A., Cemel, I.A., Ha, N., Zhang, Y., Merkl, P.E., Obermeyer, S., Stankovic-Valentin, N. and Schafmeier, T. (2017) Thiolutin is a zinc chelator that inhibits the Rpn11 and other JAMM metalloproteases. *Nature Chemical Biology*, **13**, 709-714.
12. Chan, A.N., Shiver, A.L., Wever, W.J., Razvi, S.Z., Traxler, M.F. and Li, B. (2017) Role for dithiolopyrrolones in disrupting bacterial metal homeostasis. *Proceedings of the National Academy of Sciences of the United States of America*, **114**, 2717-2722.
13. Fuchs, A.C.D., Maldoner, L., Wojtynek, M., Hartmann, M.D. and Martin, J. (2018) Rpn11-mediated ubiquitin processing in an ancestral archaeal ubiquitination system. *Nat Commun*, **9**, 2696.
14. Baell, J.B. (2011) Redox-active nuisance screening compounds and their classification. *Drug Discovery Today*, **16**, 840-841.
15. Johnston, P.A. (2011) Redox cycling compounds generate H2O2 in HTS buffers containing strong reducing reagents--real hits or promiscuous artifacts? *Curr Opin Chem Biol*, **15**, 174-182.
16. Albini, F., Bormann, S., Gerschel, P., Ludwig, V.A. and Neumann, W. (2023) Dithiolopyrrolones are Prochelators that are Activated by Glutathione. *Chemistry–A European Journal*, **29**, e202202567.
17. Khachatourians, G.G. and Tipper, D.J. (1974) In vivo effect of thiolutin on cell growth and macromolecular synthesis in Escherichia coli. *Antimicrob Agents Chemother*, **6**, 304-310.
18. Joshi, A., Verma, M. and Chakravorty, M. (1982) Thiolutin-resistant mutants of Salmonella typhimurium. *Antimicrob Agents Chemother*, **22**, 541-547.

19. Roza, J., Blanco, M.G., Hardisson, C. and Salas, J.A. (1986) Self-resistance in actinomycetes producing inhibitors of RNA polymerase. *The Journal of antibiotics*, **39**, 609-612.
20. Tipper, D.J. (1973) Inhibition of yeast ribonucleic acid polymerases by thiolutin. *J Bacteriol*, **116**, 245-256.
21. Sivasubramanian, N. and Jayaraman, R. (1976) Thiolutin resistant mutants of Escherichia coli are they RNA chain initiation mutants? *Molecular and General Genetics MGG*, **145**, 89-96.
22. Oliva, B., O'Neill, A., Wilson, J.M., O'Hanlon, P.J. and Chopra, I. (2001) Antimicrobial properties and mode of action of the pyrrothine holomycin. *Antimicrob Agents Chemother*, **45**, 532-539.
23. Mukhopadhyay, J., Das, K., Ismail, S., Koppstein, D., Jang, M., Hudson, B., Sarafianos, S., Tuske, S., Patel, J. and Jansen, R. (2008) The RNA polymerase “switch region” is a target for inhibitors. *Cell*, **135**, 295-307.
24. Wang, D. (2008) *Ensemble fluorescence resonance energy transfer analysis of RNA polymerase clamp conformation*. Rutgers The State University of New Jersey-New Brunswick.
25. Smith, A.M., Heisler, L.E., Mellor, J., Kaper, F., Thompson, M.J., Chee, M., Roth, F.P., Giaever, G. and Nislow, C. (2009) Quantitative phenotyping via deep barcode sequencing. *Genome Res*, **19**, 1836-1842.
26. Lee, A.Y., St Onge, R.P., Proctor, M.J., Wallace, I.M., Nile, A.H., Spagnuolo, P.A., Jitkova, Y., Gronda, M., Wu, Y., Kim, M.K. *et al.* (2014) Mapping the cellular response to small molecules using chemogenomic fitness signatures. *Science*, **344**, 208-211.
27. Parsons, A.B., Lopez, A., Givoni, I.E., Williams, D.E., Gray, C.A., Porter, J., Chua, G., Sopko, R., Brost, R.L., Ho, C.H. *et al.* (2006) Exploring the mode-of-action of bioactive compounds by chemical-genetic profiling in yeast. *Cell*, **126**, 611-625.
28. Perrin, D.M., Pearson, L., Mazumder, A. and Sigman, D.S. (1994) Inhibition of prokaryotic and eukaryotic transcription by the 2:1 2,9-dimethyl-1,10-phenanthroline-cuprous complex, a ligand specific for open complexes. *Gene*, **149**, 173-178.
29. Janke, C., Magiera, M.M., Rathfelder, N., Taxis, C., Reber, S., Maekawa, H., Moreno-Borchart, A., Doenges, G., Schwob, E., Schiebel, E. *et al.* (2004) A versatile toolbox for PCR-based tagging of yeast genes: new fluorescent proteins, more markers and promoter substitution cassettes. *Yeast*, **21**, 947-962.
30. Chee, M.K. and Haase, S.B. (2012) New and redesigned pRS plasmid shuttle vectors for genetic manipulation of Saccharomyces cerevisiae. *G3: Genes, Genomes, Genetics*, **2**, 515-526.
31. Huang, Z., Chen, K., Zhang, J., Li, Y., Wang, H., Cui, D., Tang, J., Liu, Y., Shi, X., Li, W. *et al.* (2013) A functional variomics tool for discovering drug-resistance genes and drug targets. *Cell reports*, **3**, 577-585.
32. Langmead, B. and Salzberg, S.L. (2012) Fast gapped-read alignment with Bowtie 2. *Nat Methods*, **9**, 357-359.
33. Li, H., Handsaker, B., Wysoker, A., Fennell, T., Ruan, J., Homer, N., Marth, G., Abecasis, G., Durbin, R. and Genome Project Data Processing, S. (2009) The Sequence Alignment/Map format and SAMtools. *Bioinformatics*, **25**, 2078-2079.
34. Robinson, D.G., Chen, W., Storey, J.D. and Gresham, D. (2014) Design and analysis of Bar-seq experiments. *G3 (Bethesda, Md.)*, **4**, 11-18.
35. Robinson, M.D., McCarthy, D.J. and Smyth, G.K. (2010) edgeR: a Bioconductor package for differential expression analysis of digital gene expression data. *bioinformatics*, **26**, 139-140.
36. de Hoon, M.J., Imoto, S., Nolan, J. and Miyano, S. (2004) Open source clustering software. *Bioinformatics*, **20**, 1453-1454.

937 37. Malik, I., Qiu, C., Snavely, T. and Kaplan, C.D. (2017) Wide-ranging and unexpected
938 consequences of altered Pol II catalytic activity in vivo. *Nucleic Acids Res*, **45**, 4431-
939 4451.
940 38. Kaplan, C.D., Jin, H., Zhang, I.L. and Belyanin, A. (2012) Dissection of Pol II trigger loop
941 function and Pol II activity-dependent control of start site selection in vivo. *PLoS*
942 *genetics*, **8**, e1002627.
943 39. Qiu, C., Erinne, O.C., Dave, J.M., Cui, P., Jin, H., Muthukrishnan, N., Tang, L.K., Babu,
944 S.G., Lam, K.C., Vandeventer, P.J. *et al.* (2016) High-Resolution Phenotypic Landscape
945 of the RNA Polymerase II Trigger Loop. *PLoS genetics*, **12**, e1006321.
946 40. Kaplan, C.D., Larsson, K.M. and Kornberg, R.D. (2008) The RNA polymerase II trigger
947 loop functions in substrate selection and is directly targeted by alpha-amanitin. *Mol Cell*,
948 **30**, 547-556.
949 41. Bolger, A.M., Lohse, M. and Usadel, B. (2014) Trimmomatic: a flexible trimmer for
950 Illumina sequence data. *Bioinformatics*, **30**, 2114-2120.
951 42. Jeronimo, C., Poitras, C. and Robert, F. (2019) Histone Recycling by FACT and Spt6
952 during Transcription Prevents the Scrambling of Histone Modifications. *Cell reports*, **28**,
953 1206-1218.e1208.
954 43. Zerbino, D.R., Johnson, N., Juettemann, T., Wilder, S.P. and Flicek, P. (2014)
955 WiggleTools: parallel processing of large collections of genome-wide datasets for
956 visualization and statistical analysis. *Bioinformatics*, **30**, 1008-1009.
957 44. Ramírez, F., Ryan, D.P., Grüning, B., Bhardwaj, V., Kilpert, F., Richter, A.S., Heyne, S.,
958 Dündar, F. and Manke, T. (2016) deepTools2: a next generation web server for deep-
959 sequencing data analysis. *Nucleic acids research*, **44**, W160.
960 45. Kent, W.J., Zweig, A.S., Barber, G., Hinrichs, A.S. and Karolchik, D. (2010) BigWig and
961 BigBed: enabling browsing of large distributed datasets. *Bioinformatics*, **26**, 2204-2207.
962 46. Birkeland, S.R., Jin, N., Ozdemir, A.C., Lyons, R.H., Jr., Weisman, L.S. and Wilson, T.E.
963 (2010) Discovery of mutations in Saccharomyces cerevisiae by pooled linkage analysis
964 and whole-genome sequencing. *Genetics*, **186**, 1127-1137.
965 47. Karim, A.S., Curran, K.A. and Alper, H.S. (2013) Characterization of plasmid burden and
966 copy number in Saccharomyces cerevisiae for optimization of metabolic engineering
967 applications. *FEMS Yeast Res*, **13**, 107-116.
968 48. Kuge, S., Jones, N. and Nomoto, A. (1997) Regulation of yAP-1 nuclear localization in
969 response to oxidative stress. *EMBO J*, **16**, 1710-1720.
970 49. Wemmie, J.A., Steggerda, S.M. and Moye-Rowley, W.S. (1997) The Saccharomyces
971 cerevisiae AP-1 protein discriminates between oxidative stress elicited by the oxidants
972 H2O2 and diamide. *Journal of Biological Chemistry*, **272**, 7908-7914.
973 50. Coleman, S.T., Epping, E.A., Steggerda, S.M. and Moye-Rowley, W.S. (1999) Yap1p
974 activates gene transcription in an oxidant-specific fashion. *Mol Cell Biol*, **19**, 8302-8313.
975 51. Kuge, S., Arita, M., Murayama, A., Maeta, K., Izawa, S., Inoue, Y. and Nomoto, A.
976 (2001) Regulation of the yeast Yap1p nuclear export signal is mediated by redox signal-
977 induced reversible disulfide bond formation. *Molecular and cellular biology*, **21**, 6139-
978 6150.
979 52. Gulshan, K., Rovinsky, S.A., Coleman, S.T. and Moye-Rowley, W.S. (2005) Oxidant-
980 specific folding of Yap1p regulates both transcriptional activation and nuclear
981 localization. *Journal of Biological Chemistry*, **280**, 40524-40533.
982 53. Alarco, A.M., Balan, I., Talibi, D., Mainville, N. and Raymond, M. (1997) AP1-mediated
983 multidrug resistance in Saccharomyces cerevisiae requires FLR1 encoding a transporter
984 of the major facilitator superfamily. *The Journal of biological chemistry*, **272**, 19304-
985 19313.

986 54. Coleman, S.T., Tseng, E. and Moye-Rowley, W.S. (1997) Saccharomyces cerevisiae
987 basic region-leucine zipper protein regulatory networks converge at the ATR1 structural
988 gene. *Journal of Biological Chemistry*, **272**, 23224-23230.
989 55. Gulshan, K. and Moye-Rowley, W.S. (2007) Multidrug resistance in fungi. *Eukaryot Cell*,
990 **6**, 1933-1942.
991 56. Meyer, Y., Buchanan, B.B., Vignols, F. and Reichheld, J.P. (2009) Thioredoxins and
992 glutaredoxins: unifying elements in redox biology. *Annu Rev Genet*, **43**, 335-367.
993 57. Winzeler, E.A., Shoemaker, D.D., Astromoff, A., Liang, H., Anderson, K., Andre, B.,
994 Bangham, R., Benito, R., Boeke, J.D., Bussey, H. *et al.* (1999) Functional
995 characterization of the S. cerevisiae genome by gene deletion and parallel analysis.
996 *Science*, **285**, 901-906.
997 58. Machado, A.K., Morgan, B.A. and Merrill, G.F. (1997) Thioredoxin reductase-dependent
998 inhibition of MCB cell cycle box activity in Saccharomyces cerevisiae. *The Journal of*
999 *biological chemistry*, **272**, 17045-17054.
1000 59. Carmel-Harel, O., Stearman, R., Gasch, A.P., Botstein, D., Brown, P.O. and Storz, G.
1001 (2001) Role of thioredoxin reductase in the Yap1p-dependent response to oxidative
1002 stress in Saccharomyces cerevisiae. *Mol Microbiol*, **39**, 595-605.
1003 60. Trotter, E.W. and Grant, C.M. (2002) Thioredoxins are required for protection against a
1004 reductive stress in the yeast Saccharomyces cerevisiae. *Mol Microbiol*, **46**, 869-878.
1005 61. Hacioglu, E., Esmer, I., Fomenko, D.E., Gladyshev, V.N. and Koc, A. (2010) The roles of
1006 thiol oxidoreductases in yeast replicative aging. *Mech Ageing Dev*, **131**, 692-699.
1007 62. Ragu, S., Dardalhon, M., Sharma, S., Iraqui, I., Buhagiar-Labarchede, G., Grondin, V.,
1008 Kienda, G., Vernis, L., Chanet, R., Kolodner, R.D. *et al.* (2014) Loss of the thioredoxin
1009 reductase Trr1 suppresses the genomic instability of peroxiredoxin tsa1 mutants. *PLoS*
1010 *One*, **9**, e108123.
1011 63. Grant, C.M., Perrone, G. and Dawes, I.W. (1998) Glutathione and Catalase Provide
1012 Overlapping Defenses for Protection against Hydrogen Peroxide in the
1013 YeastSaccharomyces cerevisiae. *Biochemical and biophysical research*
1014 *communications*, **253**, 893-898.
1015 64. Castro, F.A., Mariani, D., Panek, A.D., Eleutherio, E.C. and Pereira, M.D. (2008)
1016 Cytotoxicity mechanism of two naphthoquinones (menadione and plumbagin) in
1017 Saccharomyces cerevisiae. *PLoS One*, **3**, e3999.
1018 65. Toledano, M.B., Delaunay-Moisan, A., Outten, C.E. and Igbaria, A. (2013) Functions and
1019 cellular compartmentation of the thioredoxin and glutathione pathways in yeast. *Antioxid*
1020 *Redox Signal*, **18**, 1699-1711.
1021 66. Jung, U., Zheng, X., Yoon, S.O. and Chung, A.S. (2001) Se-methylselenocysteine
1022 induces apoptosis mediated by reactive oxygen species in HL-60 cells. *Free Radic Biol*
1023 *Med*, **31**, 479-489.
1024 67. Ravi, D. and Das, K.C. (2004) Redox-cycling of anthracyclines by thioredoxin system:
1025 increased superoxide generation and DNA damage. *Cancer Chemother Pharmacol*, **54**,
1026 449-458.
1027 68. Jimenez, A., Tipper, D.J. and Davies, J. (1973) Mode of action of thiolutin, an inhibitor of
1028 macromolecular synthesis in Saccharomyces cerevisiae. *Antimicrob Agents Chemother*,
1029 **3**, 729-738.
1030 69. Dudley, A.M., Janse, D.M., Tanay, A., Shamir, R. and Church, G.M. (2005) A global view
1031 of pleiotropy and phenotypically derived gene function in yeast. *Mol Syst Biol*, **1**, 2005
1032 0001.
1033 70. Pagani, M.A., Casamayor, A., Serrano, R., Atrian, S. and Arino, J. (2007) Disruption of
1034 iron homeostasis in Saccharomyces cerevisiae by high zinc levels: a genome-wide
1035 study. *Mol Microbiol*, **65**, 521-537.

1036 71. Ruotolo, R., Marchini, G. and Ottonello, S. (2008) Membrane transporters and protein
1037 traffic networks differentially affecting metal tolerance: a genomic phenotyping study in
1038 yeast. *Genome biology*, **9**, R67.
1039 72. Bleackley, M.R., Young, B.P., Loewen, C.J. and MacGillivray, R.T. (2011) High density
1040 array screening to identify the genetic requirements for transition metal tolerance in
1041 Saccharomyces cerevisiae. *Metallomics*, **3**, 195-205.
1042 73. Jiang, L., Cao, C., Zhang, L., Lin, W., Xia, J., Xu, H. and Zhang, Y. (2014) Cadmium-
1043 induced activation of high osmolarity glycerol pathway through its Sln1 branch is
1044 dependent on the MAP kinase kinase kinase Ssk2, but not its paralog Ssk22, in budding
1045 yeast. *FEMS Yeast Res*, **14**, 1263-1272.
1046 74. Acosta-Alvear, D., Cho, M.Y., Wild, T., Buchholz, T.J., Lerner, A.G., Simakova, O.,
1047 Hahn, J., Korde, N., Landgren, O., Maric, I. *et al.* (2015) Paradoxical resistance of
1048 multiple myeloma to proteasome inhibitors by decreased levels of 19S proteasomal
1049 subunits. *Elife*, **4**, e08153.
1050 75. Tsvetkov, P., Mendillo, M.L., Zhao, J., Carette, J.E., Merrill, P.H., Cikes, D., Varadarajan,
1051 M., van Diemen, F.R., Penninger, J.M. and Goldberg, A.L. (2015) Compromising the
1052 19S proteasome complex protects cells from reduced flux through the proteasome. *Elife*,
1053 **4**, e08467.
1054 76. Tsvetkov, P., Sokol, E., Jin, D., Brune, Z., Thiru, P., Ghandi, M., Garraway, L.A., Gupta,
1055 P.B., Santagata, S., Whitesell, L. *et al.* (2017) Suppression of 19S proteasome subunits
1056 marks emergence of an altered cell state in diverse cancers. *Proceedings of the National*
1057 *Academy of Sciences of the United States of America*, **114**, 382-387.
1058 77. Bandara, P.D., Flattery-O'Brien, J.A., Grant, C.M. and Dawes, I.W. (1998) Involvement
1059 of the Saccharomyces cerevisiae UTH1 gene in the oxidative-stress response. *Curr*
1060 *Genet*, **34**, 259-268.
1061 78. Wu, C.-Y., Bird, A.J., Winge, D.R. and Eide, D.J. (2007) Regulation of the yeast TSA1
1062 peroxiredoxin by ZAP1 is an adaptive response to the oxidative stress of zinc deficiency.
1063 *Journal of Biological Chemistry*, **282**, 2184-2195.
1064 79. Wu, C.-Y., Roje, S., Sandoval, F.J., Bird, A.J., Winge, D.R. and Eide, D.J. (2009)
1065 Repression of sulfate assimilation is an adaptive response of yeast to the oxidative
1066 stress of zinc deficiency. *Journal of Biological Chemistry*, **284**, 27544-27556.
1067 80. Wu, C.-Y., Steffen, J. and Eide, D.J. (2009) Cytosolic superoxide dismutase (SOD1) is
1068 critical for tolerating the oxidative stress of zinc deficiency in yeast. *PloS one*, **4**, e7061.
1069 81. Rudolph, H.K., Antebi, A., Fink, G.R., Buckley, C.M., Dorman, T.E., LeVitre, J., Davidow,
1070 L.S., Mao, J.I. and Moir, D.T. (1989) The yeast secretory pathway is perturbed by
1071 mutations in PMR1, a member of a Ca2+ ATPase family. *Cell*, **58**, 133-145.
1072 82. Mandal, D., Woolf, T.B. and Rao, R. (2000) Manganese selectivity of pmr1, the yeast
1073 secretory pathway ion pump, is defined by residue gln783 in transmembrane segment 6.
1074 Residue Asp778 is essential for cation transport. *The Journal of biological chemistry*,
1075 **275**, 23933-23938.
1076 83. Zencir, S., Dilg, D., Shore, D. and Albert, B. (2022) Pitfalls in using phenanthroline to
1077 study the causal relationship between promoter nucleosome acetylation and
1078 transcription. *Nat Commun*, **13**, 3726.
1079 84. Grigull, J., Mnaimneh, S., Pootoolal, J., Robinson, M.D. and Hughes, T.R. (2004)
1080 Genome-wide analysis of mRNA stability using transcription inhibitors and microarrays
1081 reveals posttranscriptional control of ribosome biogenesis factors. *Mol Cell Biol*, **24**,
1082 5534-5547.
1083 85. Sun, M., Schwalb, B., Pirkl, N., Maier, Kerstin C., Schenk, A., Failmezger, H., Tresch, A.
1084 and Cramer, P. (2013) Global Analysis of Eukaryotic mRNA Degradation Reveals Xrn1-
1085 Dependent Buffering of Transcript Levels. *Molecular Cell*, **52**, 52-62.

1086 86. D'Aurora, V., Stern, A.M. and Sigman, D.S. (1978) 1,10-Phenanthroline-cuprous ion
1087 complex, a potent inhibitor of DNA and RNA polymerases. *Biochem Biophys Res*
1088 *Commun*, **80**, 1025-1032.
1089 87. Reimann, C.W., Block, S. and Perloff, A. (1966) The Crystal and Molecular Structure of
1090 Dichloro (1, 10-phenanthroline) zinc. *Inorganic Chemistry*, **5**, 1185-1189.
1091 88. Niyogi, S.K., Feldman, R.P. and Hoffman, D.J. (1981) Selective effects of metal ions on
1092 RNA synthesis rates. *Toxicology*, **22**, 9-21.
1093 89. Lin, S.-J. and Culotta, V.C. (1996) Suppression of oxidative damage by Saccharomyces
1094 cerevisiae ATX2, which encodes a manganese-trafficking protein that localizes to Golgi-
1095 like vesicles. *Molecular and Cellular Biology*, **16**, 6303-6312.
1096 90. Portnoy, M.E., Liu, X.F. and Culotta, V.C. (2000) Saccharomyces cerevisiae expresses
1097 three functionally distinct homologues of the nramp family of metal transporters. *Mol Cell*
1098 *Biol*, **20**, 7893-7902.
1099 91. Jensen, L.T., Ajua-Alemanji, M. and Culotta, V.C. (2003) The Saccharomyces cerevisiae
1100 high affinity phosphate transporter encoded by PHO84 also functions in manganese
1101 homeostasis. *Journal of Biological Chemistry*, **278**, 42036-42040.
1102 92. Mei, Y., Jensen, L.T., Gardner, A.J. and Culotta, V.C. (2005) Manganese toxicity and
1103 Saccharomyces cerevisiae Mam3p, a member of the ACDP (ancient conserved domain
1104 protein) family. *Biochemical Journal*, **386**, 479-487.
1105 93. Reddi, A.R., Jensen, L.T., Naranuntarat, A., Rosenfeld, L., Leung, E., Shah, R. and
1106 Culotta, V.C. (2009) The overlapping roles of manganese and Cu/Zn SOD in oxidative
1107 stress protection. *Free Radic Biol Med*, **46**, 154-162.
1108 94. Walmacq, C., Kireeva, M.L., Irvin, J., Nedialkov, Y., Lubkowska, L., Malagon, F.,
1109 Strathern, J.N. and Kashlev, M. (2009) Rpb9 subunit controls transcription fidelity by
1110 delaying NTP sequestration in RNA polymerase II. *The Journal of biological chemistry*,
1111 **284**, 19601-19612.
1112 95. Pecci, L., Montefoschi, G., Musci, G. and Cavallini, D. (1997) Novel findings on the
1113 copper catalysed oxidation of cysteine. *Amino Acids*, **13**, 355-367.
1114 96. Prudent, M. and Girault, H.H. (2009) The role of copper in cysteine oxidation: study of
1115 intra- and inter-molecular reactions in mass spectrometry. *Metallomics*, **1**, 157-165.
1116 97. Fetherolf, M.M., Boyd, S.D., Taylor, A.B., Kim, H.J., Wohlschlegel, J.A., Blackburn, N.J.,
1117 Hart, P.J., Winge, D.R. and Winkler, D.D. (2017) Copper-zinc superoxide dismutase is
1118 activated through a sulfenic acid intermediate at a copper ion entry site. *The Journal of*
1119 *biological chemistry*, **292**, 12025-12040.
1120 98. Sergio, S., Pirali, G., White, R. and Parenti, F. (1975) Lipiarmycin, a new antibiotic from
1121 Actinoplanes III. Mechanism of action. *The Journal of antibiotics*, **28**, 543-549.
1122 99. Talpaert, M., Campagnari, F. and Clerici, L. (1975) Lipiarmycin: an antibiotic inhibiting
1123 nucleic acid polymerases. *Biochem Biophys Res Commun*, **63**, 328-334.
1124 100. Sonenshein, A.L. and Alexander, H.B. (1979) Initiation of transcription in vitro is inhibited
1125 by lipiarmycin. *Journal of molecular biology*, **127**, 55-72.
1126 101. Srivastava, A., Talaue, M., Liu, S., Degen, D., Ebright, R.Y., Sineva, E., Chakraborty, A.,
1127 Druzhinin, S.Y., Chatterjee, S., Mukhopadhyay, J. *et al.* (2011) New target for inhibition
1128 of bacterial RNA polymerase: 'switch region'. *Curr Opin Microbiol*, **14**, 532-543.
1129 102. Chakraborty, A., Wang, D., Ebright, Y.W., Korlann, Y., Kortkhonjia, E., Kim, T.,
1130 Chowdhury, S., Wigneshweraraj, S., Irschik, H., Jansen, R. *et al.* (2012) Opening and
1131 closing of the bacterial RNA polymerase clamp. *Science*, **337**, 591-595.
1132 103. Nayak, D., Voss, M., Windgassen, T., Mooney, R.A. and Landick, R. (2013) Cys-pair
1133 reporters detect a constrained trigger loop in a paused RNA polymerase. *Mol Cell*, **50**,
1134 882-893.
1135 104. Hein, P.P., Kolb, K.E., Windgassen, T., Bellecourt, M.J., Darst, S.A., Mooney, R.A. and
1136 Landick, R. (2014) RNA polymerase pausing and nascent-RNA structure formation are

1137 linked through clamp-domain movement. *Nature structural & molecular biology*, **21**, 794-
1138 802.
1139 105. Werner, F. (2012) A nexus for gene expression-molecular mechanisms of Spt5 and
1140 NusG in the three domains of life. *J Mol Biol*, **417**, 13-27.
1141
1142

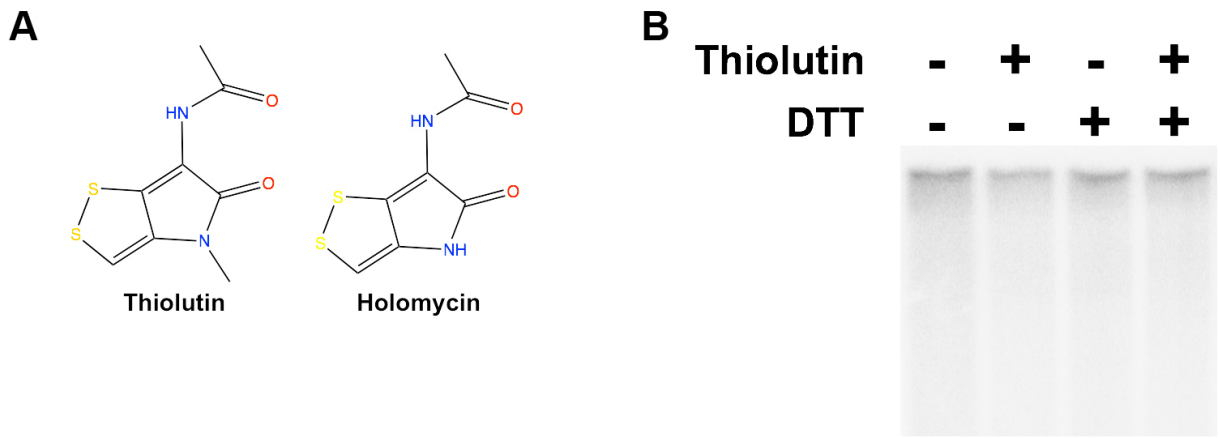

1143
1144 **Figure 1. Thiolutin or reduced thiolutin alone fails to inhibit purified yeast Pol II *in vitro*.**
1145 (A) Thiolutin and holomycin structures.
1146 (B) Thiolutin, or thiolutin treated with equimolar DTT, show no inhibition of Pol II transcription *in*
1147 *vitro*. Transcription activity assay was performed with ssDNA as the template and NTPs,
1148 including ^{32}P labeled UTP. The transcribed ^{32}P containing RNA was separated from free ^{32}P
1149 UTPs on 10% polyacrylamide gels for visualization. Experiments were performed with at least
1150 three times, and a representative experiment is shown.
1151

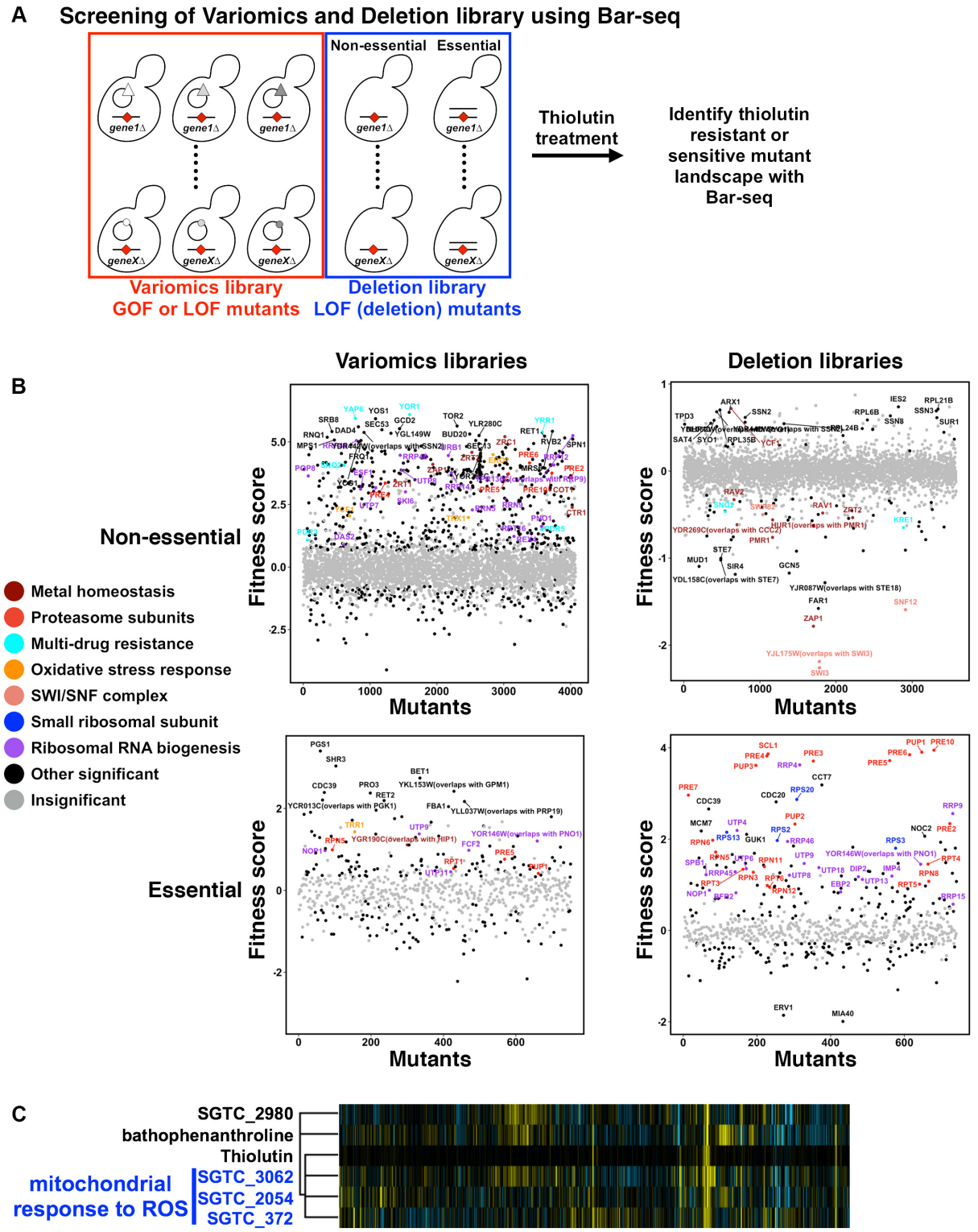

Figure 2. Mutations in diverse cellular pathways confer resistance/sensitivity to thiolutin. (A) Four libraries (Variomics libraries for non-essential or essential genes, Deletion libraries for non-essential or essential genes) were used for screening thiolutin resistant or sensitive mutants. Changes in abundance in the library was detected by deep sequencing of the PCR amplicon of the barcode region (Bar-seq). Variomics libraries consist of random gene variants

1158 and can be used to screen for both Gain-of-Function (GOF) and Loss-of-Function (LOF) alleles,
1159 whereas “Deletion” libraries consist of single-gene-deleted mutants that can be used to screen
1160 for complete LOF mutants.
1161 (B) Different thiolutin resistant or sensitive mutant classes are revealed in the Bar-seq based
1162 screenings of pooled Variomics and Deletion libraries.
1163 (C) Thiolutin induced phenotypic profile in the pooled deletion libraries co-clusters with drugs
1164 with signature of “mitochondrial response to ROS” (26) and bathophenanthroline, a metal
1165 chelator. 4683 deletion mutants’ responses (in columns) to 3356 compounds (in rows) were
1166 used for hierarchical clustering, but only the thiolutin closely correlated compounds are shown in
1167 this figure for clarity. Resistant strains: yellow; Sensitive strains: blue.
1168

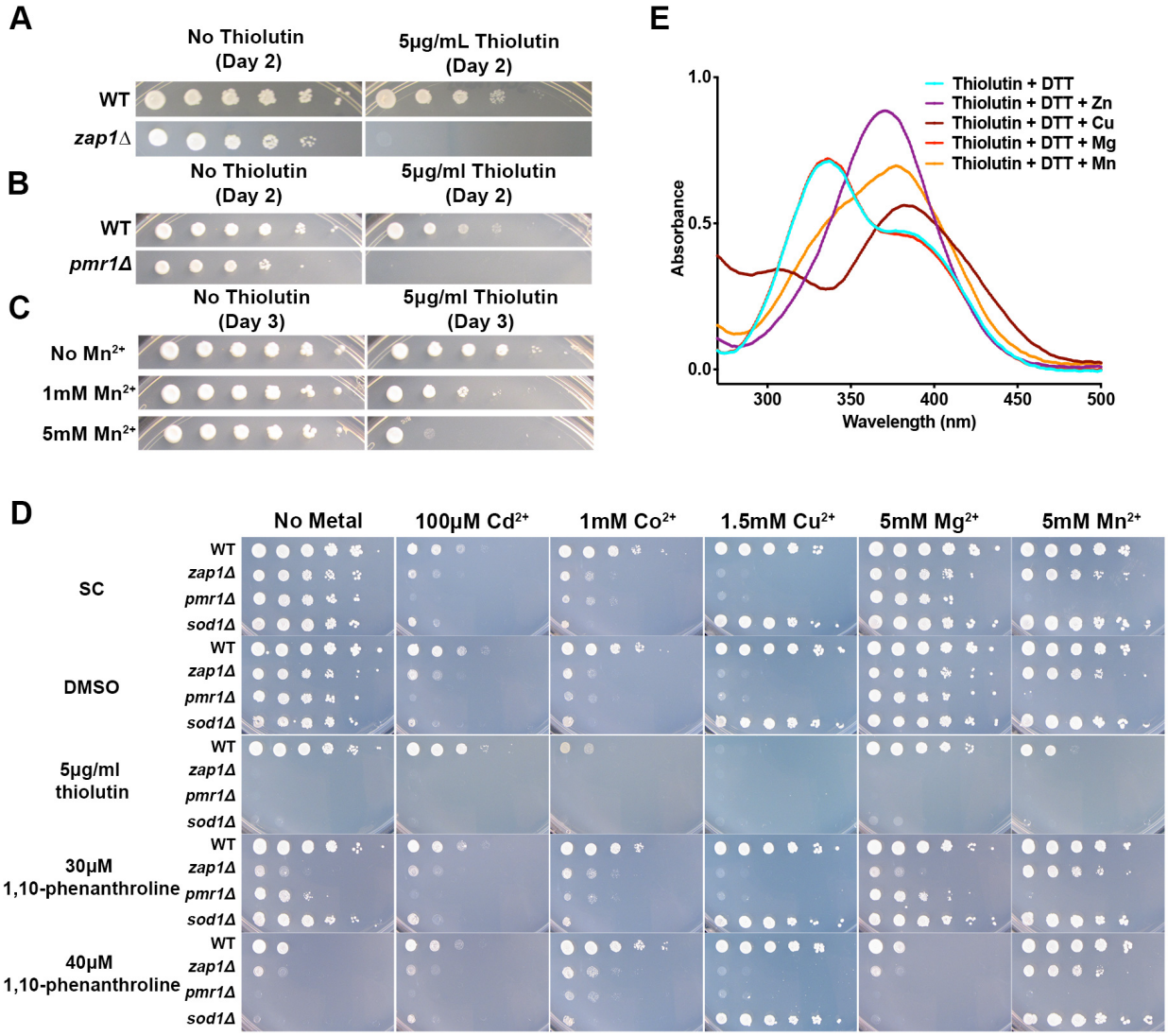

Figure 3. Divalent metals cations appear to alter thiolutin sensitivity *in vivo* and interact with reduced thiolutin *in vitro*. (A-D) 10-fold serial dilutions of yeast strains spotted onto different types of media to examine thiolutin sensitivity. (A) *zap1*Δ is hypersensitive to thiolutin. (B) *pmr1*Δ is hypersensitive to thiolutin. (C) Mn^{2+} supplementation exacerbates WT yeast sensitivity to thiolutin. (D) Distinct sensitivities of thiolutin and 1,10-phenanthroline to Co^{2+}, Cu^{2+}, and Mn^{2+} and differential interactions with gene deletions. (E) Reduced thiolutin was incubated with a selection of divalent metal cations and UV absorbance was analyzed. Zn^{2+} , Mn^{2+}, and Cu^{2+}, but not Mg^{2+}, interact with reduced thiolutin, as evident by alteration of the UV spectra of reduced thiolutin.

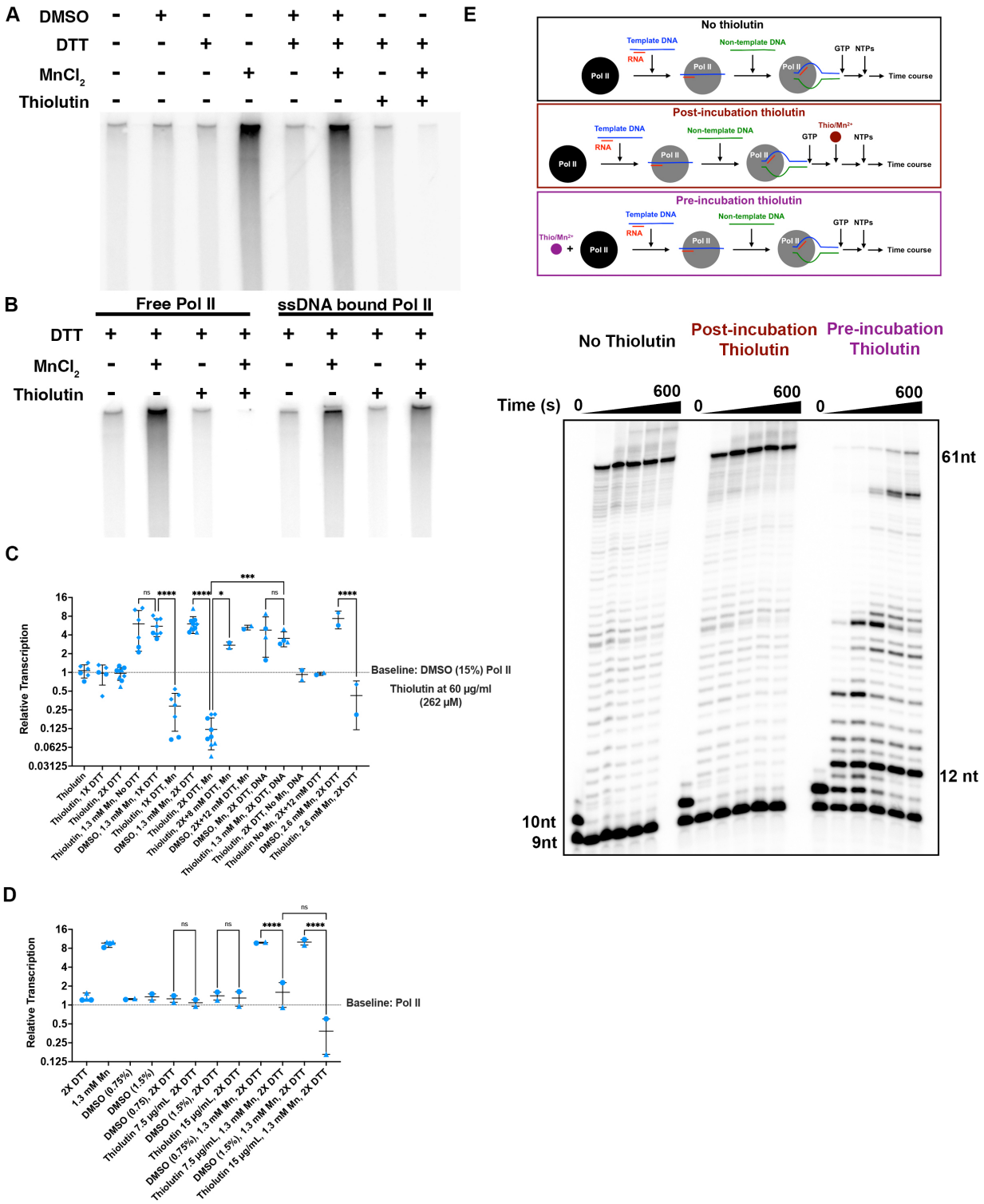

Figure 4. Apparent thiolutin/Mn^{2+} complex inhibits Pol II transcription *in vitro* and *in vivo*. (A) Thiolutin requires both DTT (reductant) and Mn^{2+} to inhibit Pol II transcription *in vitro*. A representative of multiple experiments is shown. Quantifications of this and a wide range of experimental conditions for thiolutin inhibition are shown in Figure S10. (B) Pre-binding to DNA renders Pol II resistant to Thiolutin/Mn^{2+} complex. This gel is representative of multiple independent experiments (Quantifications shown in Figure S10). (C) Quantification of thiolutin

1187 inhibition under a number of experimental conditions. Thiolutin (60 µg/mL) inhibition of Pol II
1188 requires DTT and Mn2+ and is blocked by pre-incubation of Pol II with DNA or with excess (12
1189 mM) DTT added after Pol II treatment with thiolutin. All reactions are compared to baseline for
1190 individual Pol II in particular experiment, which is activity of Pol II plus vehicle (15% DMSO
1191 final). Different symbols indicate three independent Pol II purifications used in experiments.
1192 Note that variability in fraction of Pol II inhibited by thiolutin appears to track with Pol II
1193 purification (▲● Pol II consistently more inhibited than ◆). Error bars are mean +/- Standard
1194 Deviation. Statistical analysis for selected pairs is one-way ANOVA with multiple comparisons
1195 controlling for False Discovery Rate (0.01) (method of Benjamini, Krieger, Yekutieli). **** = p<
1196 0.0001, *** = p< 0.0002. * p< 0.0332. (D) Quantification of thiolutin inhibition at lower
1197 thiolutin/DMSO concentrations and additional controls. All reactions are compared to baseline
1198 for individual Pol II in particular experiment, which is activity of Pol II in absence of drug or
1199 vehicle. Different symbols indicate two separate Pol II purifications (symbols here match Pol II
1200 purifications in (C). Statistical analysis for selected pairs is one-way ANOVA with multiple
1201 comparisons controlling for False Discovery Rate (0.01) (method of Benjamini, Krieger,
1202 Yekutieli). **** = p< 0.0001. (E) In vitro elongation assay for Thiolutin-treated Pol II. (Top)
1203 Schematic indicates three assembly pathways for making elongation complexes on nucleic acid
1204 scaffolds in the absence of thiolutin, incubation with thiolutin after elongation complex assembly,
1205 or before elongation complex assembly. (Bottom) Thio/Mn^{2+} inhibited Pol II can be directly
1206 assembled into a distinct and slow elongating complex, but only if Pol II is treated with thiolutin
1207 prior to complex assembly. Two experimental replicates were performed, and a representative
1208 replicate is shown. Time points for addition of NTPs were 0, 10, 30, 120, 300, and 600 seconds.
1209

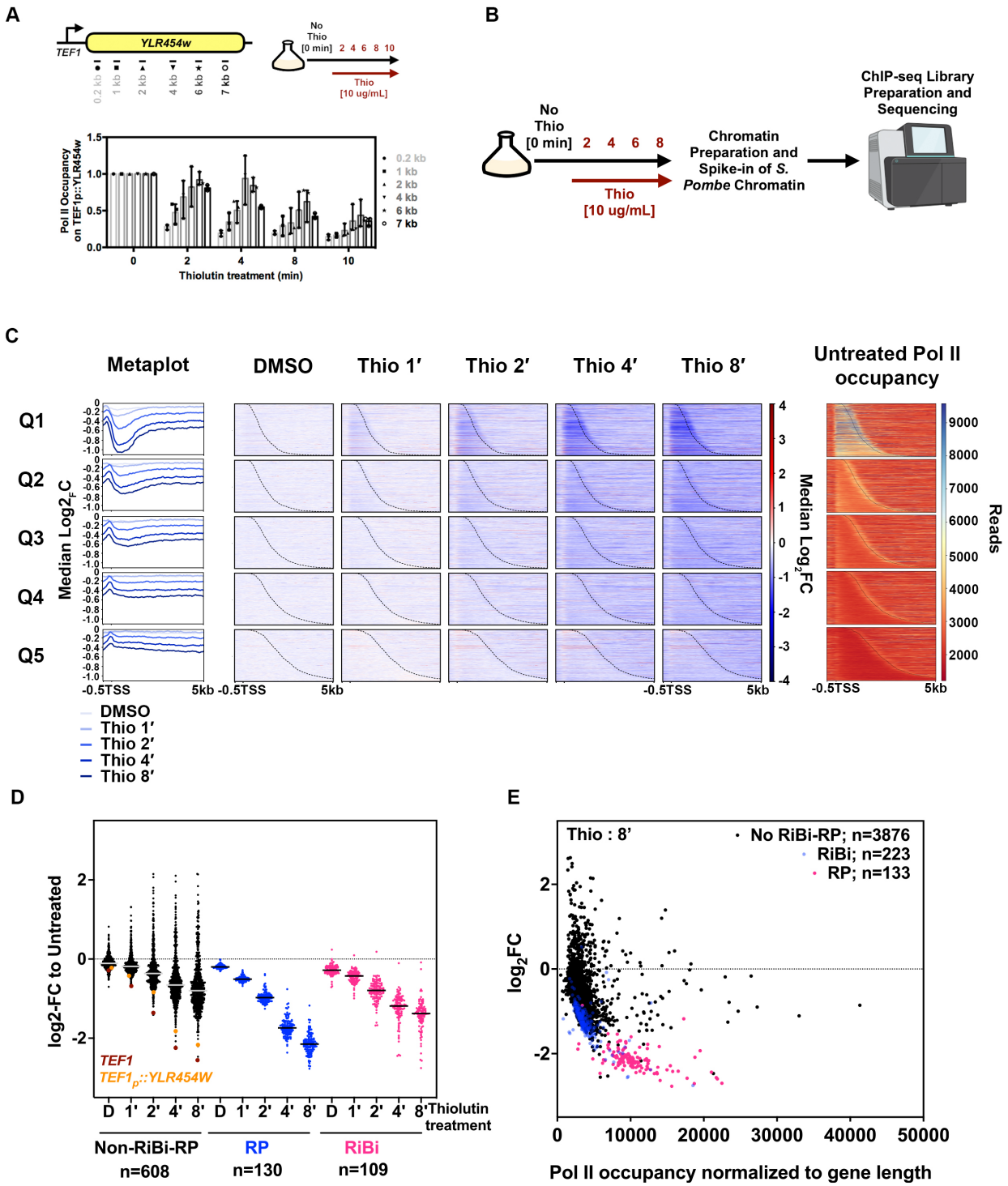

Figure 5. Thiolutin reduces Pol II occupancy genome wide. (A) Thiolutin inhibits Pol II occupancy at a *TEF1* promoter-driven *YLR454W* reporter *in vivo.* Schematic indicates positions of PCR primers for chromatin immunoprecipitation-quantitative PCR (ChIP-qPCR) for a FLAG-tagged Rpb3 subunit of Pol II at a reporter gene representing a long transcription unit. Thiolutin (10μg/mL) was added to cells for indicated times prior to crosslinking for ChIP. Three experimental replicates were performed, and error bars represent standard deviation of the

1217 mean. (B) Schematic of Pol II ChIP-seq experiment thiolutin treatment for the indicated times
1218 (control sample with addition of vehicle DMSO was for 8 minutes treatment). (C) Genome-wide
1219 decreases of Pol II occupancy at genes separated into quintile based on normalized Pol II
1220 occupancy in untreated cells from highest (Q1) to lowest (Q5). Quintiles are ~846 genes each.
1221 Genes are rank ordered from shortest to longest with annotated gene 3′-ends indicated with the
1222 dashed line. (D) The majority of genes show decreases in Pol II occupancy as determined by
1223 fold change in normalized Pol II occupancy per base within each gene. Genes separated by
1224 class indicate that ribosomal protein (RP) genes show greater Pol II decreases than do
1225 ribosomal biogenesis (RiBi) than do other highly expressed genes in Q1. (E) Decrease in Pol II
1226 occupancy (y axis) shows some correlation with initial occupancy levels (x-axis) with RP genes
1227 showing special sensitivity to thiolutin treatment.
1228

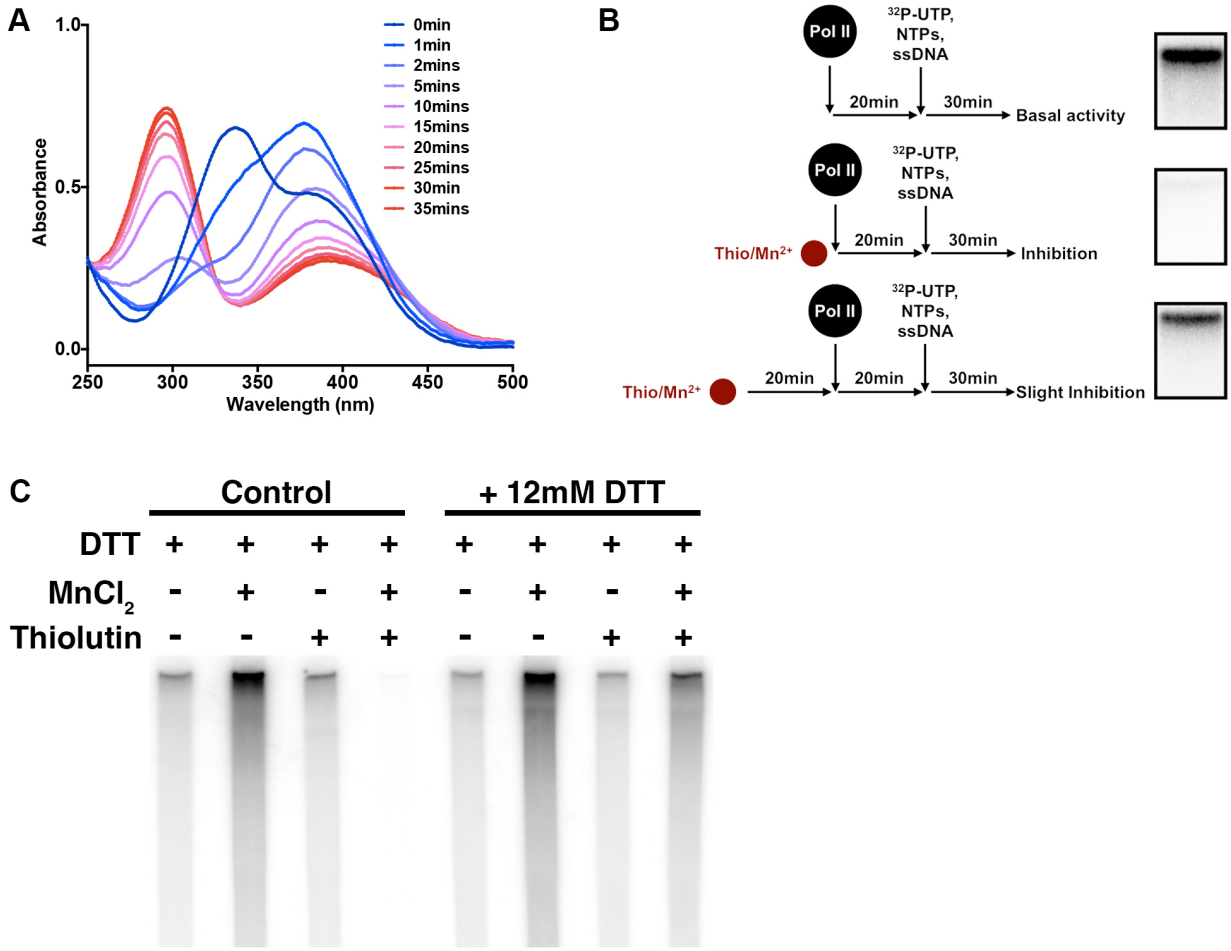

Figure 6. The apparent Thiolutin/Mn^{2+} complex is unstable in solution but stable in Pol II. (A) Time course of changing UV spectra of reduced thiolutin treated with Mn^{2+}. Reduced thiolutin (blue, 0 min) was treated with equivalent molar Mn^{2+}, and the UV spectra was acquired at different time points. Spectra over time was colored in a series of gradient from blue to red. Three experimental replicates were performed, and a representative replicate is shown. (B) Thio/Mn^{2+} lost inhibitory activity after 20 mins in solution though immediately treated Pol II remains inhibited. Two experimental replicates were performed and consistent. One replicate is shown. (C) Thio/Mn^{2+} can be reversed by excess DTT. Excess of DTT was added after 20 minutes of Pol II inhibition by Thio/Mn^{2+}. DTT was at 12 mM during thiolutin treatment. Two replicates under these exact conditions were performed, and a representative replicate is shown. Results are representative of additional experiments performed under slightly different conditions.

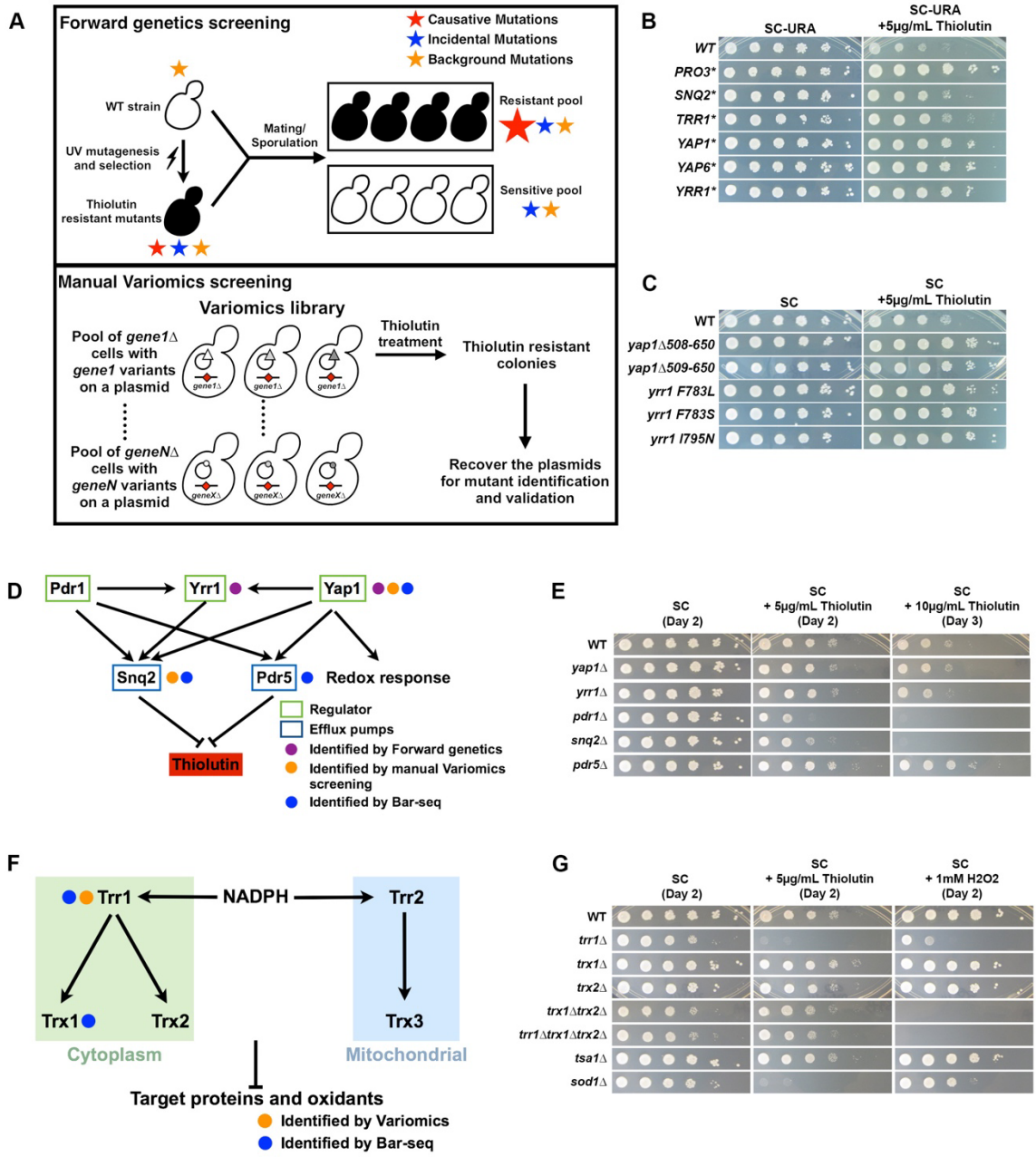

Figure S1. Mutations in multiple drug resistance (MDR) and oxidative stress responses (OSR) pathways alters cellular sensitivity to thiolutin.

(A) Schematic diagram of the two independent genetic screens for thiolutin resistant mutants. Top: For the forward genetic screening, WT yeast strain (CKY457) was UV mutagenized and screened for thiolutin resistant mutants, and mutations were identified by whole-genome sequencing after bulk segregant analysis. Bottom: The gene-specific Variomics libraries consist of many mutants for a given gene in a yeast cell pool, and Variomics libraries for > 4000 genes were further pooled together for thiolutin resistance screening. Plasmids from the validated thiolutin resistant mutants were recovered for Sanger sequencing to identify both the gene and potential mutations. (B) Reproducibly-isolated thiolutin-resistant mutants from the forward genetics and manual Variomics screening. (C) Forward genetics isolated thiolutin-resistant alleles of *YAP1* and *YRR1*. (D) Schematic diagram summarizing a partial regulatory network of multiple drug resistance, with isolated resistant mutants indicated. The reported or hypothesized functional interactions are indicated by pointed (activation) or blunt-end (inhibition) arrows. (E) Distinct thiolutin sensitivity of MDR deficient mutants. *pdr1*Δ and *snq2*Δ are

sensitive to thiolutin, whereas other tested MDR deficient strains retain resistance. (F) Schematic diagram summarizing the regulatory network of thioredoxin system in yeast, with isolated resistant mutants indicated. (G) Distinct thiolutin sensitivity of some OSR deficient mutants.

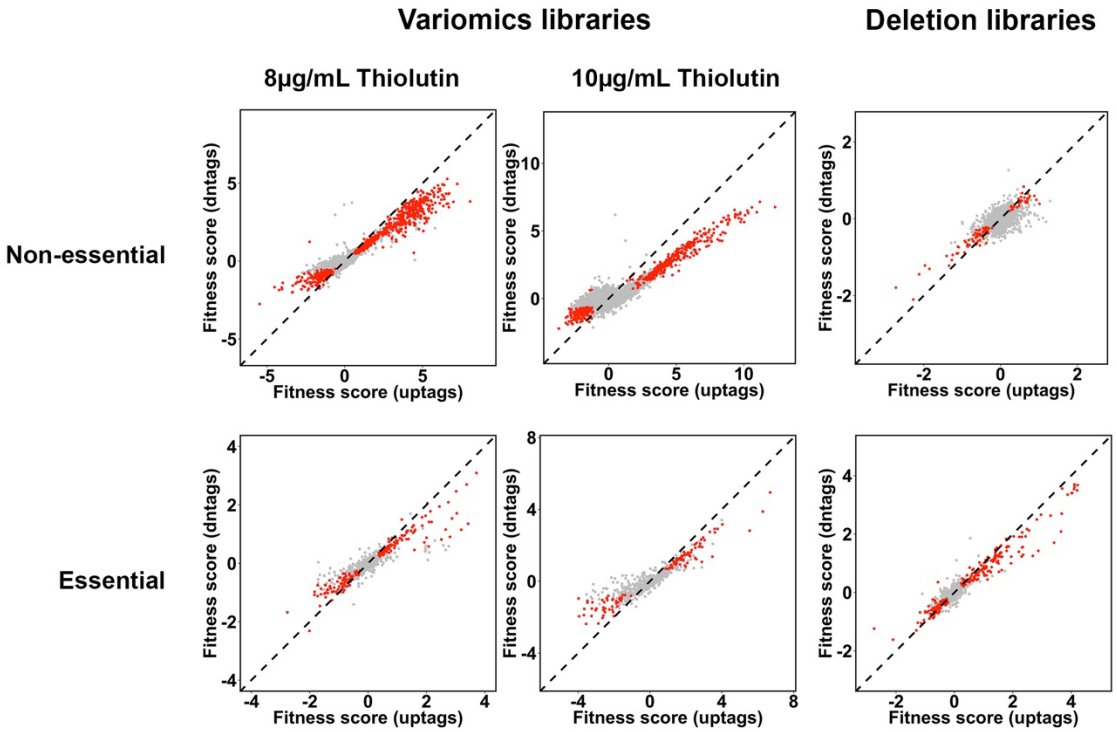

Figure S2. Correlation between uptag and downtags results in Bar-seq. Xyplots showing the fitness score (log2 of the fold change in relative abundance) computed from both uptag and downtags. Mutants are declared significantly resistant or sensitive in both tags are colored in red, whereas others are colored in light grey. y=x is shown as a dashed line.

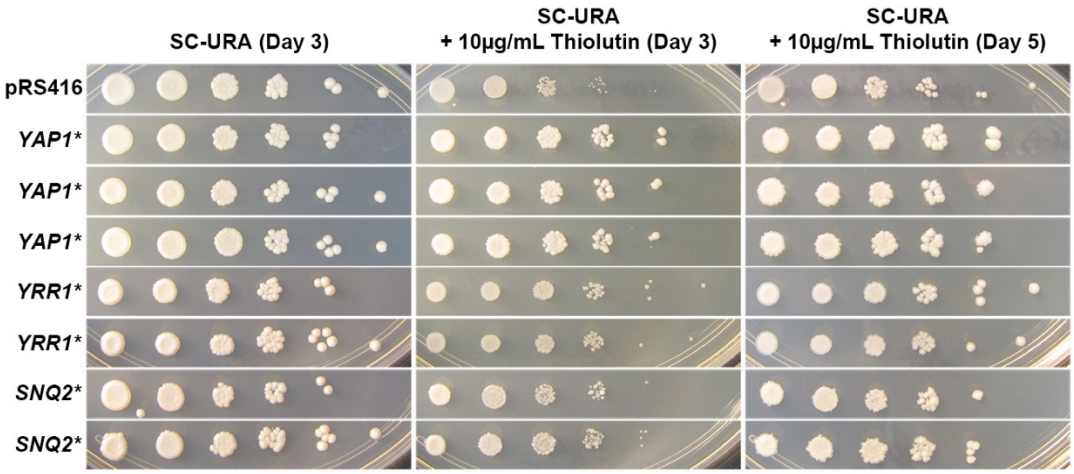

Figure S3. Isolated thiolutin resistant MDR Variomics candidates are dominant or dosage dependent. Plasmids recovered from the Variomics candidates are transformed into WT yeast strain along with an empty vector (pRS416) control, thiolutin resistance are assessed for at least two independent transformants.

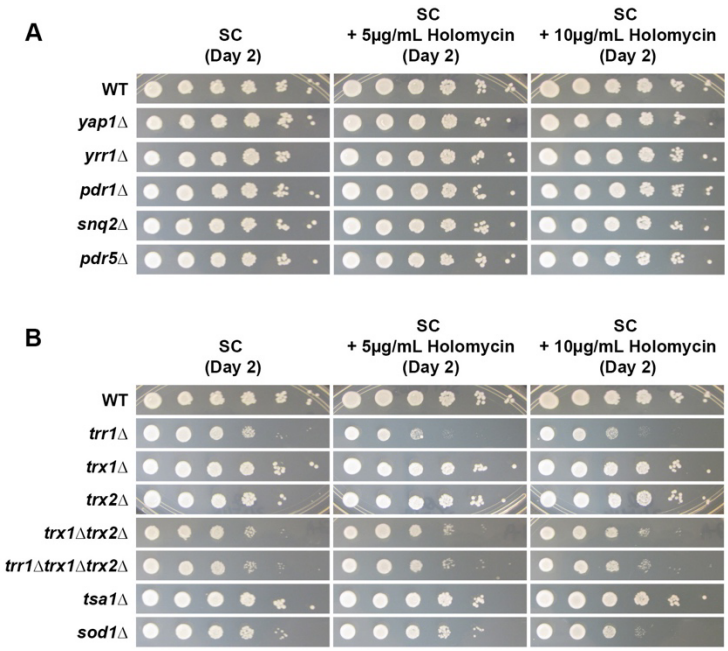

Figure S4. Tested MDR and OSR deficient mutants do not confer the same hypersensitivity to holomycin as to thiolutin.
(A) Plate growth assays of serially diluted MDR deficient mutants on SC complete media with indicated holomycin concentration. (B) Plate growth assays of serially diluted OSR deficient mutants on SC complete media with indicated holomycin concentration.

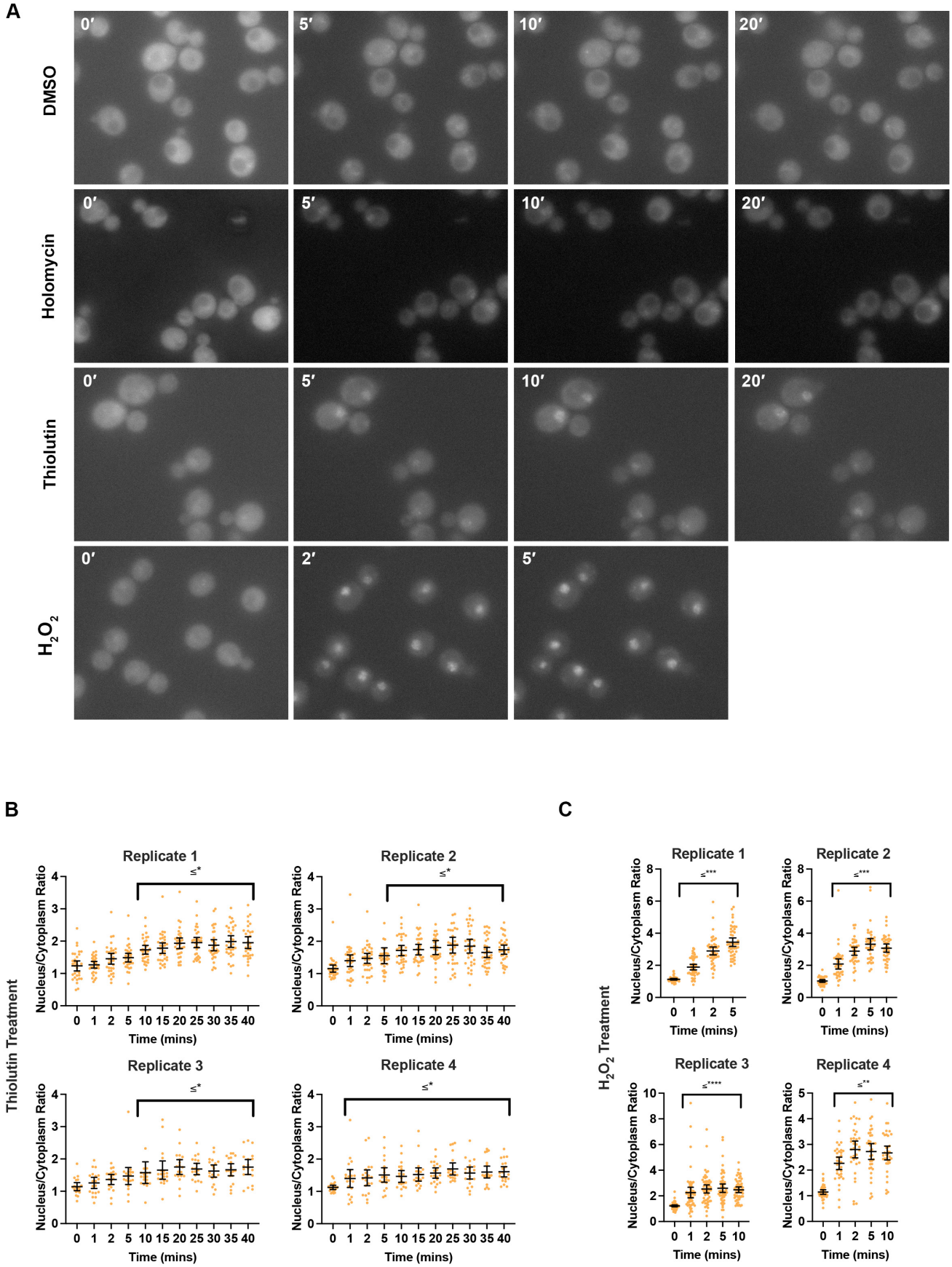
A
DMSO
Holomycin
Thiolutin
H_2O_2
0′
5′
10′
20′
2′
B
Thiolutin Treatment
Replicate 1
Replicate 2
Replicate 3
Replicate 4
Nucleus/Cytoplasm Ratio
Time (mins)
≤*
C
H_2O_2 Treatment
≤***
≤****
≤**

Figure S5. Thiolutin induces nuclear localization of the redox-sensitive Yap1 transcription activator.
(A) Representative images of Yap1 relocalization to the nucleus after thiolutin or peroxide treatment. An EGFP-taggedYap1 strain was treated with 1% DMSO (control), 10μg/mL thiolutin, 10μg/mL holomycin, or 0.4mM H_2O_2. GFP fluorescence was monitored after treatment at the indicated time points. (B) Quantification of nuclear/cytoplasmic EGFP signal ratio for individual cells after 10μg/mL thiolutin treatment, for four independent biological replicates. Background was subtracted when nuclear and cytoplasmic signal were quantified. Error bars represent mean +/- the 95% confidence interval. (C) Quantification of nuclear/cytoplasmic EGFP signal ratio for individual cells after 0.4mM H_2O_2 treatment, in four different biological replicates. Quantification and error bars are as described in (B). Statistical test was Friedman's paired test for each time point versus the 0 minute point for relevant cells (Dunn's correction for multiple comparisons). Adjusted P-values indicated as *,**,***, **** were * ≤0.0332, ** ≤0.0021, *** ≤0.00002, **** <0.00001. " ≤ *" indicates all P values were at * or below.

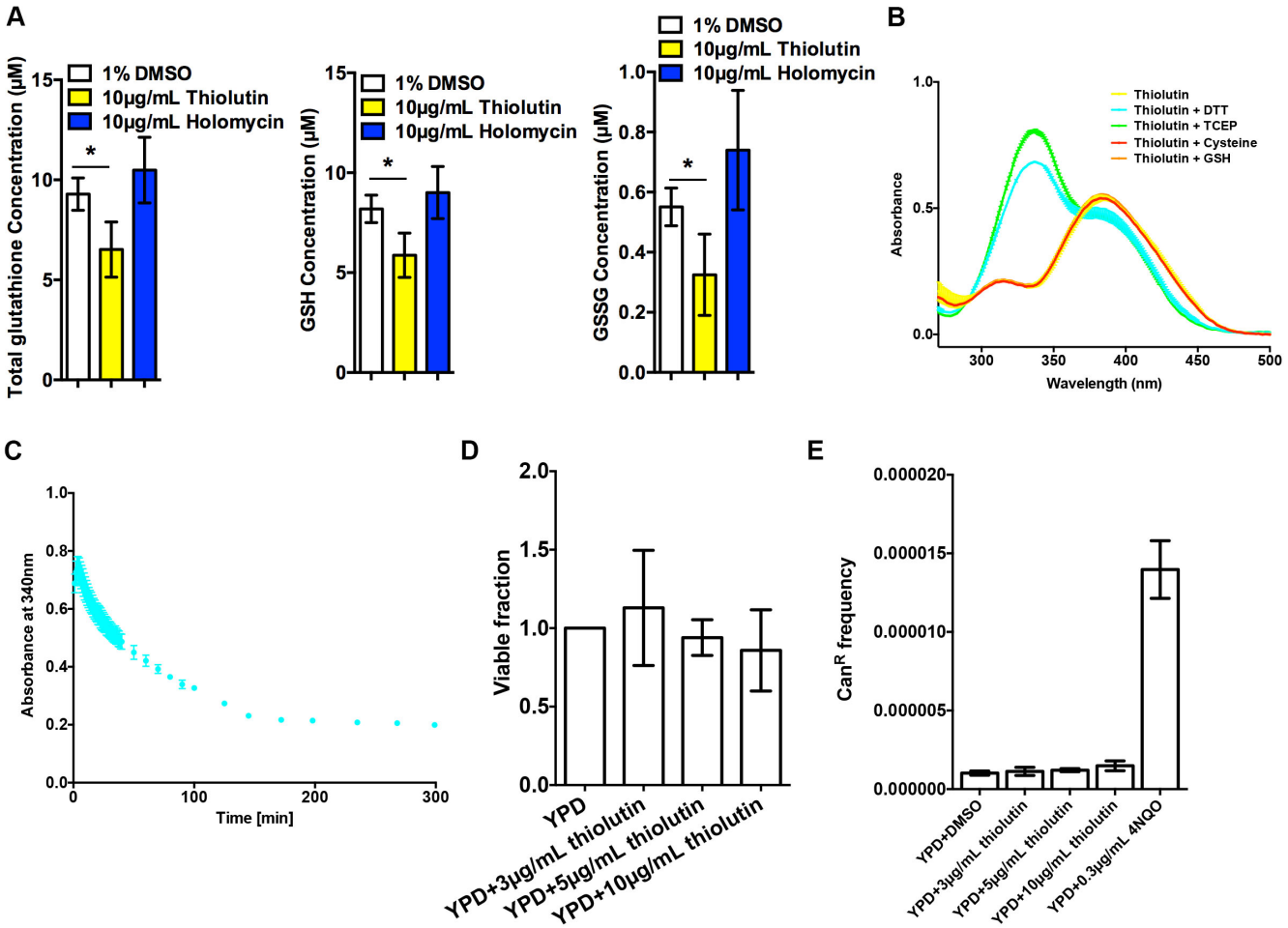

Figure S6. Thiolutin appears to induce oxidative stress partially through redox cycling.
(A) Thiolutin depletes total glutathione *in vivo*. Growing WT yeast cultures are washed and treated with indicated conditions at 30˚C for an hour. Reduced glutathione (GSH) and total glutathione are measured in three independent replicates, and the oxidized glutathione (GSSG) are calculated. The error bars represent standard deviation of the mean. *p≤0.01 (Two-tailed paired t-test). (B) Thiolutin can be reduced by DTT and TCEP, but not glutathione or cysteine *in vitro*. The reactions were performed in 100mM phosphate buffer (pH 6.5) with equivalent molar reductant with thiolutin. UV spectra were measured 1 minute after the reactions. Three independent replicates were performed and the error bars represent standard deviation of the mean. (C) Reduced thiolutin is spontaneously re-oxidized when exposed to air. The reactions were performed as described in Figure 3D, and UV absorbance at

340nm plotted over a time course. Three independent replicates were performed and the error bars represent standard deviation of the mean. (D) Acute exposure to thiolutin does not affect yeast viability. (E) Thiolutin does not cause DNA damage, as measured by mutation frequency at *CAN1* gene.

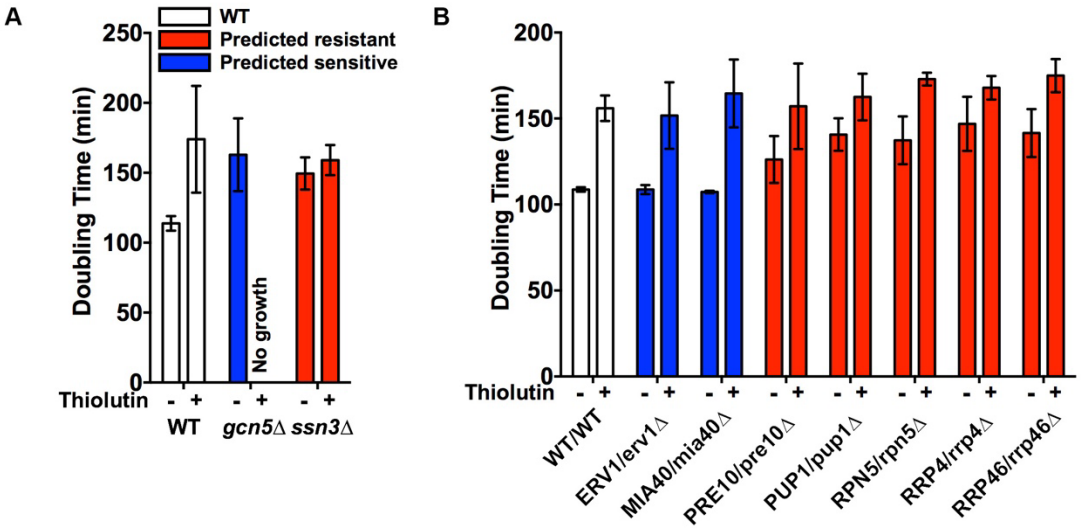

Figure S7. Validation of several statistically significantly resistant or sensitive mutants. Mutants were reconstructed in haploid BY4741 or diploid BY4743 backgrounds originally used to construct the deletion libraries, and mid-log growth at 30˚C was assessed using a Tecan plate reader. Three independent repeats were performed and the error bars represent standard deviation of the mean. We failed to validate the observed slight sensitivity in *ERV1/erv1*Δ and *MIA40/mia40*Δ, two strains that were statistically significantly sensitive in Bar-seq but the sensitivity was very slight.

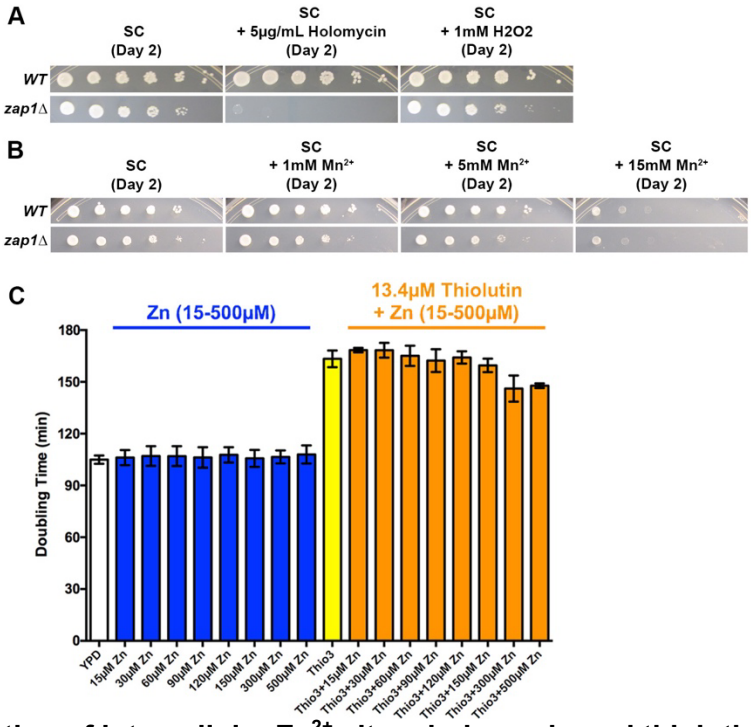

Figure S8. Modulation of intracellular Zn^{2+} alters holomycin and thiolutin sensitivity.
(A) *zap1*Δ is hypersensitive to holomycin, but not H_2O_2. (B) *zap1*Δ doesn't confer sensitivity to Mn^{2+}. (C) Zn^{2+} supplementation partially suppresses thiolutin sensitivity. Doubling time were derived from growth curves measured by a Tecan plate reader. Three independent repeats were performed and the error bars represent standard deviation of the mean.

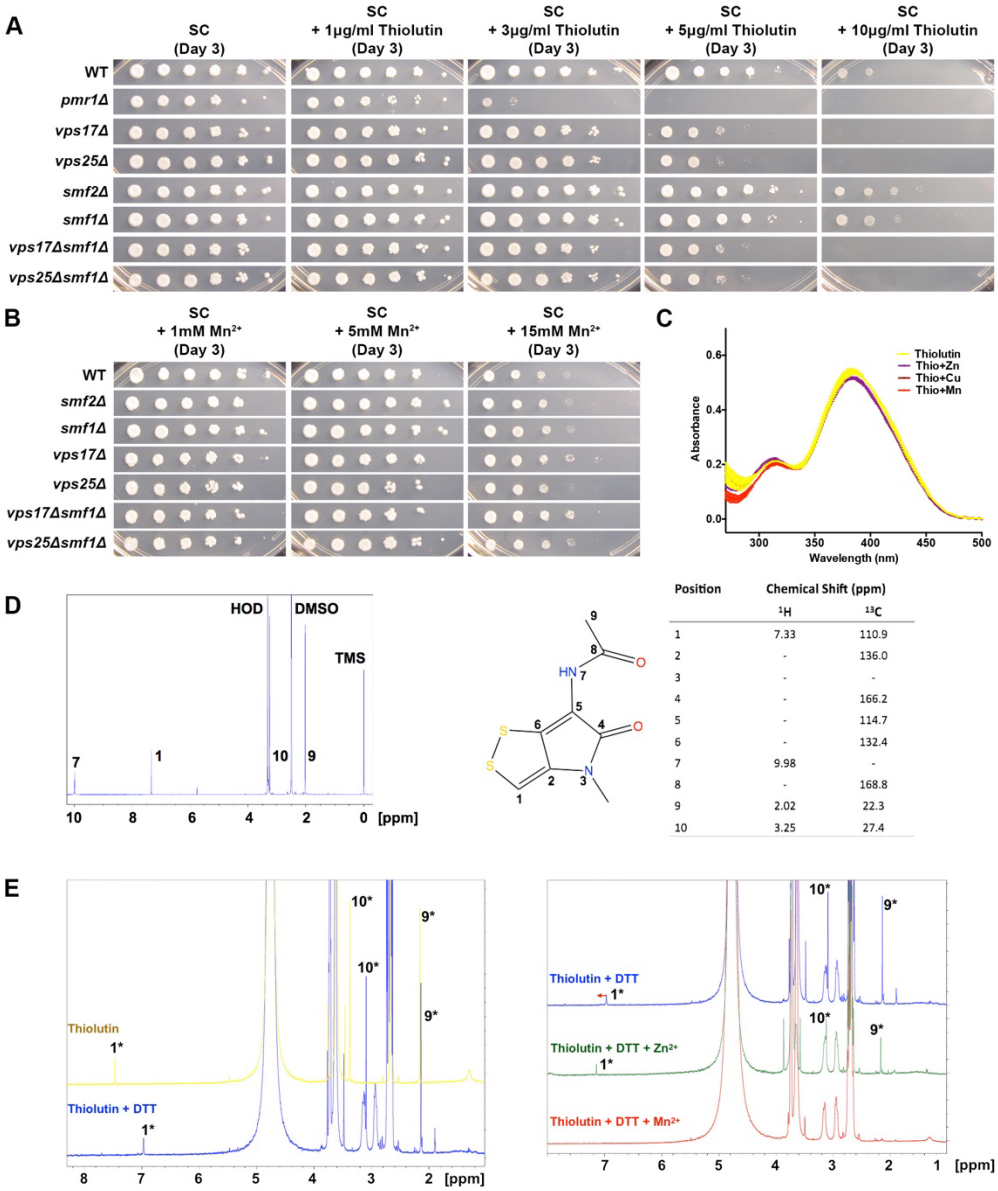

Position	Chemical Shift (ppm)	
	^{1}H	^{13}C
1	7.33	110.9
2	-	136.0
3	-	-
4	-	166.2
5	-	114.7
6	-	132.4
7	9.98	-
8	-	168.8
9	2.02	22.3
10	3.25	27.4

Figure S9. Mn^{2+} may modulate the sensitivity to reduced thiolutin *in vivo* and directly interact with thiolutin *in vitro*.

(A) *pmr1*Δ is hyper-sensitive to thiolutin, while *vps17*Δ and *vps25*Δ appear to confer thiolutin sensitivity independent of Smf1-dependent Mn^{2+} trafficking. (B) *vps17*Δ, *vps25*Δ, *smf1*Δ and *smf2*Δ do not confer sensitivity to Mn^{2+} in our strain background and assays. (C) Zn^{2+}, Cu^{2+} and Mn^{2+} do not alter the UV absorbance profile of thiolutin. (D) Assigned 1H-NMR spectrum of thiolutin. (E) Left: Change in thiolutin spectra immediately after reduction by DTT; Right: Changes in DTT-reduced thiolutin chemical shifts after addition of Zn^{2+} (diamagnetic) or Mn^{2+} (paramagnetic).

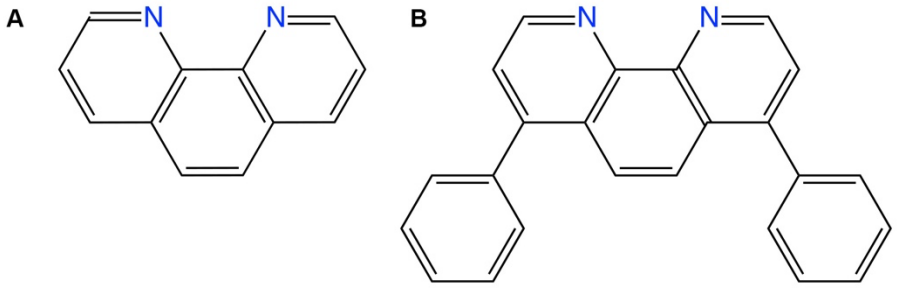

Figure S10. Structures of 1,10-phenanthroline and bathophenanthroline.
(A) 1,10-phenanthroline. (B) bathophenanthroline

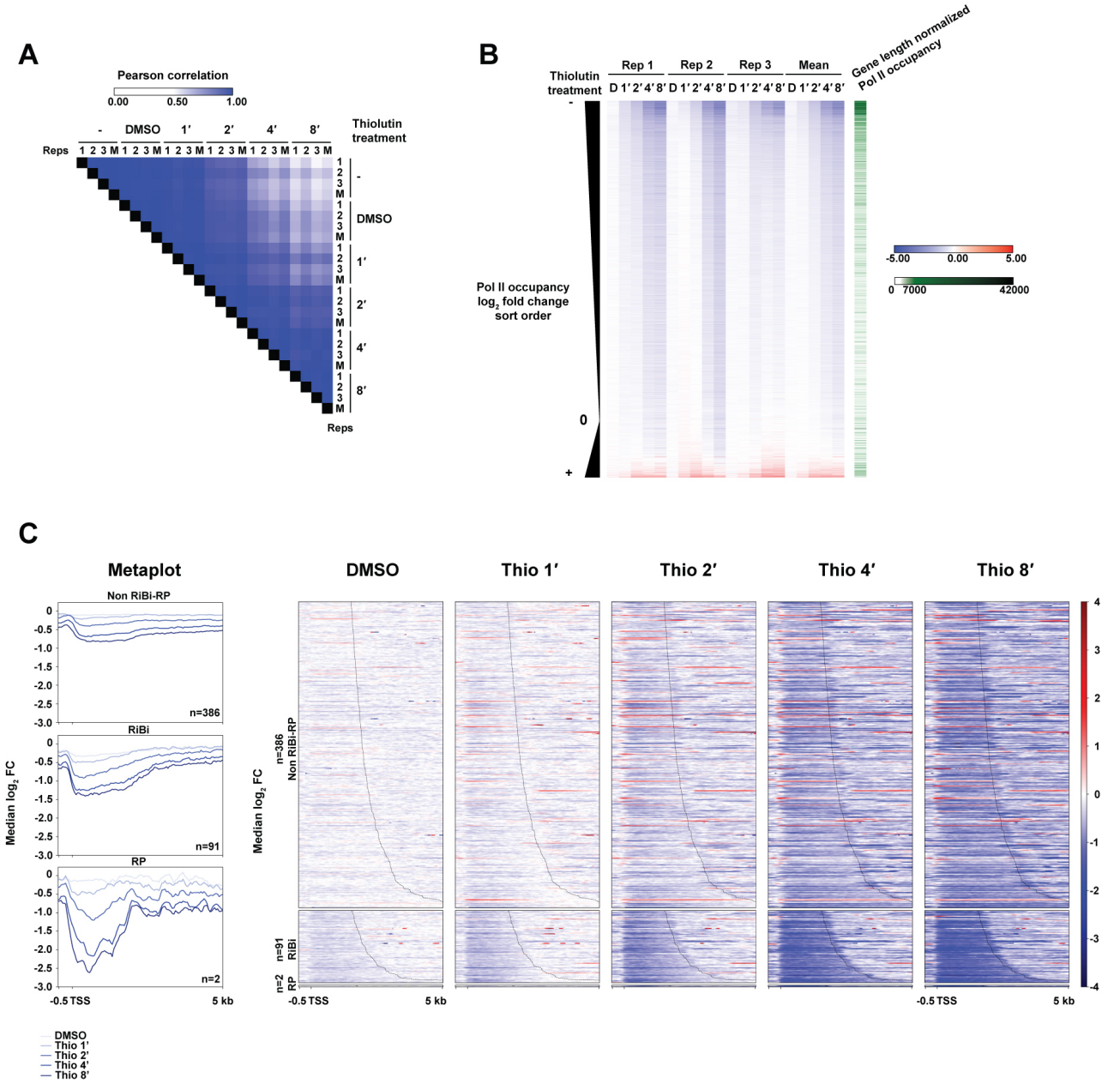

Figure S11. ChIP-seq for Pol II from thiolutin treated yeast. (A) Biological replicates of thiolutin treatment are reproducible. Heat map of Pearson r values for normalized Pol II occupancy/gene length for annotated yeast genes. Three biological replicates ("1","2","3") and the mean of the replicates ("M") for untreated cells (-), DMSO-treated control cells, and thiolutin treatment (10µg/mL) for 1, 2, 4, or 8 minutes are arranged in a heat map. Pearson r values are indicated by the color scale for comparison of samples on the x and y axes. (B) Yeast genes rank ordered from greatest decrease in Pol II occupancy to greatest increase for biological replicates with $\log_2$ fold change in spike-in normalized Pol II occupancy/gene length shown in a heat map. (C) Yeast genes from the top 40% based on Pol II occupancy in untreated cells that are ≥1.5 kb in length were divided into non-RP/RiBi genes (n=386), RiBi genes (n=91), and RP genes (n=2) and ordered by length (Right panels). Median $\log_2$ fold change in Pol II occupancy between treatment (DMSO or thiolutin) and untreated conditions is shown. Left panels are the metaplots for change in Pol II occupancy over time of thiolutin treatment.